

Simulation of St. Louis, Missouri, Land Use Impacts on Thunderstorms

CHRISTOPHER M. ROZOFF AND WILLIAM R. COTTON

Department of Atmospheric Science, Colorado State University, Fort Collins, Colorado

JIMMY O. ADEGOKE

Department of Geosciences, University of Missouri at Kansas City, Kansas City, Missouri

(Manuscript received 31 May 2002, in final form 16 December 2002)

ABSTRACT

A storm-resolving version of the Regional Atmospheric Modeling System is executed over St. Louis, Missouri, on 8 June 1999, along with sophisticated boundary conditions, to simulate the urban atmosphere and its role in deep, moist convection. In particular, surface-driven low-level convergence mechanisms are investigated. Sensitivity experiments show that the urban heat island (UHI) plays the largest role in initiating deep, moist convection downwind of the city. Surface convergence is enhanced on the leeward side of the city. Increased momentum drag over the city induces convergence on the windward side of the city, but this convergence is not strong enough to initiate storms. The nonlinear interaction of urban momentum drag and the UHI causes downwind convection to erupt later, because momentum drag over the city regulates the strength of the UHI. In all simulations including a UHI, precipitation totals are enhanced downwind of St. Louis. Topography around St. Louis also affects storm development. There is a large sensitivity of simulated urban-enhanced convection to the details of the urban surface model.

1. Introduction

Many observational studies indicate that rainfall patterns in and downwind of cities are modified. With substantial evidence that St. Louis, Missouri, enhanced convective storms in its vicinity, the large cooperative project, Metropolitan Meteorological Experiment (METROMEX), took place over St. Louis from 1971 to 1975 (Braham 1976; Changnon 1981). METROMEX confirmed that deep, moist convection is enhanced in and downwind of St. Louis. Since METROMEX, observations indicate that population growth in several cities was associated with an increasing frequency of thunderstorms around those cities (Balling and Brazel 1987; Jaurequi and Romales 1996). Case studies over Atlanta, Georgia, carried out by Bornstein and Lin (2000), concluded that some storms may be initiated by the urban heat island (UHI) downwind of Atlanta and that storms approaching Atlanta may diverge around the peripheries of the city.

Modeling studies support observations of increased convection resulting from the urban surface. Simulations conducted by Hjelmfelt (1982) indicate that the heat island and the increased roughness of the St. Louis

surface enhance boundary layer convection. Thielen et al. (2000) used a simple parameterization for surface sensible and latent heat flux and urban roughness within a two-dimensional (2D) model. Sensitivity experiments showed that variations in the surface parameters, especially sensible heat flux, affected the development of precipitation over Paris, France. Baik and Kim (2001) used a 2D mesoscale model to illustrate how prescribed atmospheric heating sources representative of UHIs affected dry and moist convection. They showed that the distance of nonlinear convective cells from the heating source decreases and the strength of the convection increases as the basic-state flow decreases and the heating amplitude increases. More recently, Craig and Bornstein (2002) carried out 3D mesoscale simulations for a case study and showed that the UHI induces convergence and convection. In all cases cited above, the surface representation was simple or nonexistent.

The current study applies a 3D cloud-resolving mesoscale model to examine some hypotheses explaining urban-enhanced convection. Most hypotheses include storms enhanced through low-level convergence driven by the UHI and urban surface roughness, and by anthropogenic aerosols. The reasons why storms are enhanced over urban areas are obscured by complexities in the boundary layer. The current study investigates low-level convergence-related mechanisms. Because observations from METROMEX indicated orographic

Corresponding author address: Christopher M. Rozoff, Department of Atmospheric Science, Colorado State University, Fort Collins, CO 80523.
E-mail: rozoff@atmos.colostate.edu

TABLE 1. A summary of the basic model configuration.

Category	Options
Governing equations	3D, nonhydrostatic, compressible
Vertical coordinate	Terrain-following σ_z
Grid stagger and configuration	Arakawa-C grid; three fixed, nested grids
Time differencing	Leapfrog and forward time difference
Turbulence closure	K from deformation (Smagorinsky) scaled by stability
Lower boundary	LEAF-2 with Town Energy Budget
Upper boundary	Rigid lid with modified Rayleigh friction layer
Lateral boundaries	Klemp and Wilhelmson (1978), nudged from outer-grid meteorological state
Microphysics	One-moment bulk microphysics
Cumulus parameterization	None
Radiation	Chen and Cotton (1983)

enhancement of precipitation (Changnon 1981), topographic impacts on convection are also studied in the current modeling application.

This study is an extension of previous modeling work in that sophisticated boundary conditions accounting for urban geometry are employed at the surface. In addition, nonlinear processes are studied. A real case study is employed over St. Louis on a day when isolated, outflow-dominant storms occurred. Such a situation emphasizes storm-forcing mechanisms resulting near the surface. In section 2, the numerical cloud-resolving mesoscale model, initialization procedures, and the experimental design are described. Section 3 describes a convective case study over St. Louis and shows general model performance. Two surface schemes are compared against data and the superior scheme is chosen for sensitivity experiments. To study the convective forcing mechanisms, factor-separation technique results for sensitivity experiments are provided in section 4. Last, section 5 offers a summary of findings and conclusions.

2. Model configuration and experimental design

The Regional Atmospheric Modeling System (RAMS), version 4.3, is used to simulate the atmosphere for this study (Cotton et al. 2003). RAMS is cloud-resolving and nonhydrostatic, and it contains sophisticated microphysics, turbulence, and radiation components. Table 1 summarizes many of the schemes and methods used in the current study.

The Land Ecosystem–Atmosphere Feedback-2 (LEAF-2) (Walko et al. 2000) model is the surface–vegetation–atmosphere transfer (SVAT) package included in RAMS. LEAF-2 currently contains 30 different land surface types, most of which are defined in the Biosphere–Atmosphere Transfer Scheme (BATS) (Dickinson et al. 1986). Within a grid cell, multiple patches can be used to represent the heterogeneity of vegetation classes. For urban land, the leaf area index and vegetation fractional coverage are minimized and

the roughness length is increased to approximate the effects of the barren, rough city surface.

The Town Energy Budget (TEB) (Masson 2000) generalized canyon model replaces the LEAF-2 urban class-30 parameterization to accurately represent the 3D urban surface and roughness sublayer in a mesoscale model. It provides to the first model level quantities such as sensible heat flux, latent heat flux, two momentum covariances, albedo, and emissivity. RAMS obtains TEB's fluxes for each grid cell at the first atmospheric level as an urban patch contribution, at which point the fluxes are averaged with LEAF-2 nonurban patches. The current study uses no variations in the parameters of TEB to approximate the average characteristics of urban land use over St. Louis.

a. Grid configuration

Three fixed grids are employed in the current study. The inner two grids are two-way interactive nested grids. The fine grid (grid 3) is intended to explicitly resolve deep, moist convection. Grid 3 has grid spacing of 1.5 km, 102×102 horizontal grid points, and a time step of 3.75 s. The coarser grids simulate the general synoptic and mesoscale setting. Grid 2 has 7.5-km grid spacing with 92×82 horizontal grid points and a time step of 15 s. Grid 1 has 37.5-km grid spacing with 50×40 horizontal grid points and a time step of 60 s. The three grids are centered over St. Louis. There are 40 vertical σ_z layers that are stretched from spacings of 0.1–0.8 km in the first 0–7.5 km of the atmosphere and maintained at spacings of 0.8 km for heights above 7.5 km. The total depth of the model atmosphere is 22 km.

b. Initialization of atmospheric fields

RAMS is initialized and nudged with gridded analyses from the Eta Model Data Assimilation System (EDAS), as described in Rogers et al. (1996). An isentropic analysis is used to interpolate the EDAS data into RAMS data every 3 h. Temperature, pressure, humidity, and wind components are interpolated into RAMS for initial conditions of grids 1 and 2. Grid-2 initial conditions are then interpolated into grid 3. Noise in the beginning of the model integration is prevented by setting the initial vertical velocity to zero without balance constraints on the initial mass and horizontal wind fields.

c. Initialization of surface fields

Land use and land cover (LULC) for grids 1 and 2 are based on the Advanced Very High Resolution Radiometer (AVHRR)-derived Olson Global Ecosystem (OGE) land cover data from the U.S. Geological Survey (USGS) Earth Resources Observation System (EROS) Data Center (Lee 1992). These data cover the conterminous United States and have a spatial resolution of

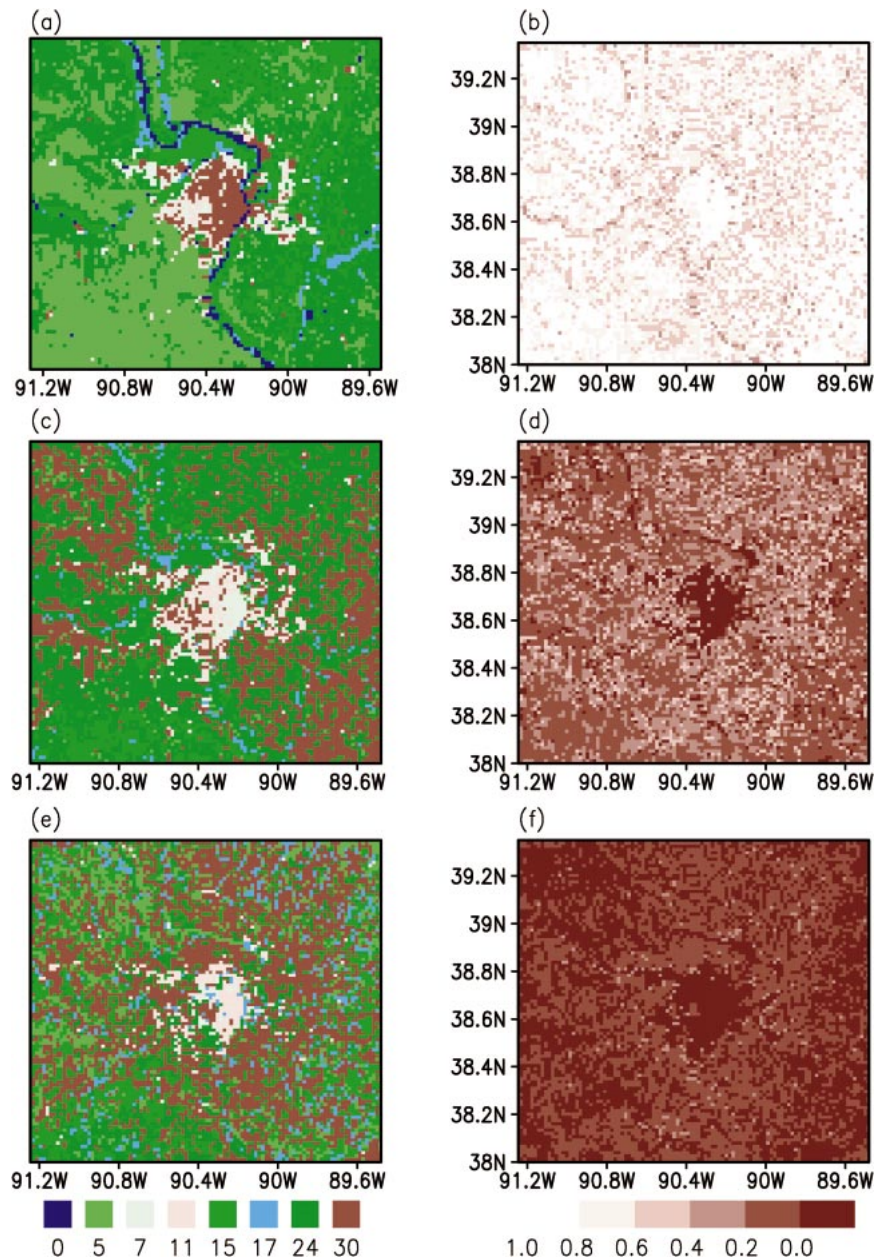


FIG. 1. LULC data used in study for the (a) first two patches (first patch is reserved for open water), (c) third patch, and (e) fourth patch. (Here, 0 = open water, 5 = deciduous broadleaf trees, 7 = short grass, 11 = suburban, 15 = crop/mixed farming, 17 = bog/marsh, 24 = wooded grassland, and 30 = urban.) Also shown is the fraction of the grid cell covered by land use in the (b) first and second patch, (d) third patch, and (f) fourth patch.

1 km. RAMS maps the data into BATS categories in LEAF-2.

To more accurately represent the heterogeneous urban surface and other local physiographic features within grid 3, we use a 1-km-resolution version of the 30-m Landsat Thematic Mapper (TM) National Land Cover Data (NLCD). The 1-km data contain the aggregated percentage of the area occupied by each of the 21 NLCD land cover types in the original 30-m TM data. These

data are a vast improvement over the standard RAMS LULC data because the critical information on the fractional area of each land cover type is computed from the full-resolution data and is retained in the aggregated version. In this study we use one water patch and three other patches for the three most dominant land types in each grid cell, thus, accounting for almost all of the variability in the NLCD.

Figure 1 represents the LULC around St. Louis and

TABLE 2. Dominant LULC LEAF-2 biophysical parameters. Here, α = albedo, ϵ = emissivity, LAI = leaf area index, f = fractional coverage of vegetation, z_o = roughness length (m), and z_d = displacement height (m).

LEAF-2 class	α	ϵ	LAI	f	z_o	z_d
Water	0.14	0.99	0.0	0.0	0.0	0.1
Deciduous broadleaf	0.20	0.95	6.0	0.8	0.8	15.0
Short grass	0.26	0.96	2.0	0.8	0.02	0.2
Suburban	0.19	0.93	4.6	0.77	0.65	5.1
Cropland	0.20	0.95	6.0	0.85	0.06	0.7
Bog/marsh	0.12	0.98	6.0	0.8	0.03	1.0
Wooded grassland	0.18	0.96	5.0	0.8	0.51	3.6
Urban	0.15	0.9	4.8	0.74	0.8	1.1

patch fractional grid cell coverage for grid 3. High-density residential areas, highways, and commercial and industrial zones are categorized by the urban class 30 in RAMS. For the most dominant patch, urban class 30 shows up in the center of the domain. Elsewhere, some suburban areas (class 11) show up around the edge of the city. In these areas, LEAF-2 biophysical parameters are optimized to account for the building morphology and a significant amount of vegetation. Deciduous broadleaf forests, short grass, farmland, wooded grassland, and marshes along the rivers predominantly cover the surrounding rural land.

The LULCs in LEAF-2 each possess unique biophysical parameters to simulate their effects on the atmosphere. As a result, the momentum, heat, and moisture flux vary from one land class to another. Some of the key biophysical parameters for the most dominant grid-3 LULCs are provided in Table 2.

When TEB is used, information is needed to describe building and road materials and average geometry of the urban area. Roofs and walls are composed of dense concrete (layer 1), aerated concrete (layer 2), and insulation (layer 3). Roads are made up of asphalt for the top layer (layer 1), and dry soil beneath (layers 2 and 3). Most of the construction material values are found in Masson (2000) and Oke (1988). Other TEB parameters are subjectively determined from recent aerial photographs of St. Louis. For example, an average building height of 15 m, with building and canyon aspect ratios of unity, are reasonable for the average St. Louis "class 30" land. Roughness length is 0.8 m, a value typical of urban/suburban areas. Table 3 summarizes important TEB parameters.

Eleven soil layers are used in all grids. Soil moisture and temperatures are initialized heterogeneously with the EDAS data, although the EDAS- and RAMS-type soil parameters are not spatially dependent. When TEB is applied, three layers compose the underground, as described above.

TABLE 3. Urban characteristics used by TEB.

Parameter	Value
Fractional area covered by buildings	0.5
Fractional area covered by roads	0.5
Building height (m)	15
Building aspect ratio (height/length)	1
Canyon aspect ratio (height/width)	1
Roughness length (m)	0.8
Roof layers 1, 2, and 3 thicknesses (cm)	5, 40, 5
Wall layers 1, 2, and 3 thicknesses (cm)	2, 12.5, 2
Road layers 1, 2, and 3 thicknesses (cm)	5, 10, 100
Roof, wall, and road albedos	0.15, 0.25, 0.08
Roof, wall, and road emissivities	0.9, 0.85, 0.94

d. Experiments

The surface factors related to urban-enhanced convection hypotheses are examined using sensitivity experiments. Attention is paid to individual contributions of each factor variation and the possible interactions between factors.

Simulations with and without each of the following factors are performed: urban radiative and energy fluxes, urban roughness, and local topography. When the urban factors are ignored, the respective surface parameters of the dominant surrounding rural land use are implemented in their place. In this case, dense urban LULC becomes cropland (class 15), and suburban land becomes wooded grassland (class 24). It is important to note that rural landscape variability may still impact convection. The simulation without the local topography has its topography interpolated from grid 1 (Fig. 2b). Avoiding a completely flat grid 1 minimizes terrain disparities in larger-scale synoptic weather. Small-scale variability in grid-3 topography (Fig. 2a), believed to possibly influence local rainfall, is not present in the simulation with smoothed topography.

We vary momentum flux to simulate the effects of roughness. Extreme care must be taken to separate the effects of roughness. Turbulent fluxes of heat also depend on roughness length. Therefore, for experiments neglecting urban energy balance, but including the effects of urban roughness, the turbulent momentum flux is calculated through TEB's formulation. The turbulent heat and radiative fluxes are computed considering the rural biophysical parameters, including rural roughness lengths.

On the other hand, two urban simulations involve momentum flux computed with rural roughness lengths. Here, all other urban surface layer fluxes are computed considering the urban roughness lengths. When varying the roughness length, the dense urban and suburban land areas must be adapted. For urban roughness runs, the urban and suburban areas have z_o set to 0.8 and 0.65 m, respectively. For rural roughness runs, urban and suburban land roughness lengths are set to 0.06 and 0.51 m, respectively.

To accomplish the goal of true factor separation, the

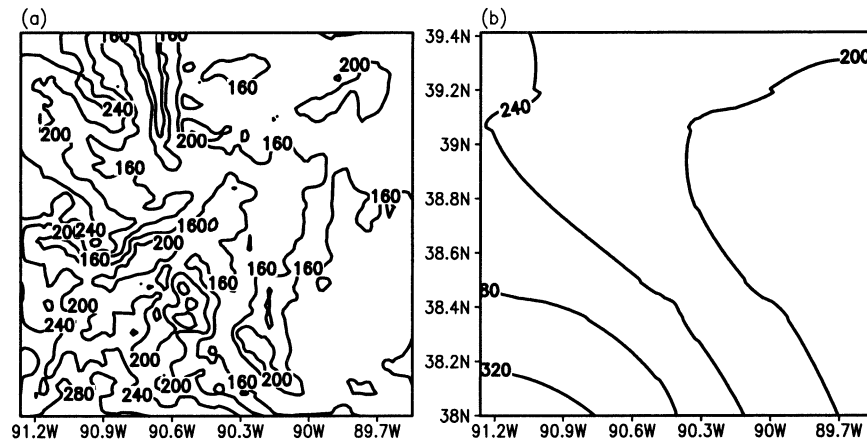


FIG. 2. (a) Regular and (b) smoothed topography over St. Louis (m) for grid 3.

technique of Stein and Alpert (1993) is employed. Because three factor variations are used, eight simulations must be carried out. Then, true contributions from each variation and the synergies between factors may be perceived. The experiments are summarized in Table 4. An additional experiment (L2), using the original LEAF-2 urban parameterization, is included to be compared with the control simulation (f_{123}), which incorporates TEB. The difference fields necessary to separate individual and interactive contributions are listed in Table 5.

3. 8 June 1999 simulation results

This study employs a real case study day with a number of convective events in the area of St. Louis. Certain criteria are considered so that the simulations are as generalized as possible. Results are sought to be comparable with observations reported in METROMEX. In METROMEX, “air mass” storms were found to be 116% more frequent downwind of St. Louis than in rural areas (Changnon 1981). This percentage increase in frequency was much greater than the enhancement in any of the other categories of storms. Following these results, the current numerical experiments are derived

from a convective situation that occurred in an environment devoid of large-scale forcing and where scattered, outflow-dominant storms developed over and around St. Louis. We identify storms on 8 June 1999 as “ordinary storms.”

a. 8 June 1999 weather

The St. Louis area experienced heavy thunderstorms on 8 June 1999. Storms initiated in the early afternoon and lasted throughout the evening. According to Storm Prediction Center storm report data, large hail fell within the county warning area and considerable wind damage to buildings and trees was reported in the city of St. Louis. Locally heavy rains also resulted from some of the storms. Despite the severity of these storms, their isolated and transient nature, along with the relatively weak flow aloft, made this event suitable for the study of urban-enhanced storms. The weak southwesterly mean tropospheric flow and a relatively warm and moist surface identified with this event certainly yielded results within the climatic conditions of METROMEX. Huff and Vogel (1978) found that 43% of storms af-

TABLE 4. Summary of experiments performed. The “Rural” and “Urban” specifications indicate which type of surface layer calculation is used. Unless noted otherwise, all urban computations are performed with TEB.

Experiment	Energy balance	Topography	Momentum flux
f_0	Rural	Smoothed	Rural
f_1	Urban	Smoothed	Rural
f_2	Rural	Unsmoothed	Rural
f_3	Rural	Smoothed	Urban
f_{12}	Urban	Unsmoothed	Rural
f_{23}	Rural	Unsmoothed	Urban
f_{13}	Urban	Smoothed	Urban
f_{123}	Urban	Unsmoothed	Urban
L2	Urban (LEAF-2)	Unsmoothed	Urban (LEAF-2)

TABLE 5. Summary of the difference fields and the mechanisms leading to that field.

Symbol	Difference	Mechanism
\hat{f}_0	f_0	Nonurban, nontopographic
\hat{f}_1	$f_1 - f_0$	Urban energy fluxes
\hat{f}_2	$f_2 - f_0$	Topographic
\hat{f}_3	$f_3 - f_0$	Urban momentum flux
\hat{f}_{12}	$f_{12} - (f_1 + f_2) + f_0$	Urban energy flux and topographic interaction
\hat{f}_{23}	$f_{23} - (f_2 + f_3) + f_0$	Urban momentum flux and topographic interaction
\hat{f}_{13}	$f_{13} - (f_1 + f_3) + f_0$	Urban energy flux and urban momentum flux interaction
\hat{f}_{123}	$f_{123} - (f_{12} + f_{13} + f_{23}) + (f_1 + f_2 + f_3) - f_0$	Interaction of all factors

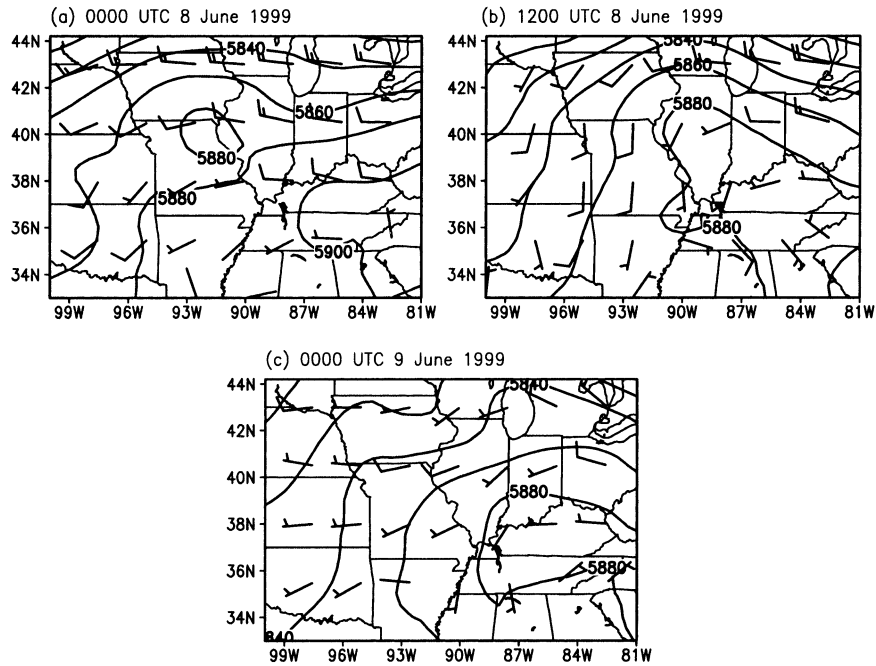


FIG. 3. EDAS 500-hPa geopotential heights (m) with wind vectors (m s^{-1}) at (a) 0000 and (b) 1200 UTC 8 Jun, and (c) 0000 UTC 9 Jun 1999.

fecting the St. Louis area came from the southwest and west-southwest during METROMEX. Hence, this episode is capable of providing general results applicable to previously published data.

The synoptic situation on 8 June 1999 involved an anticyclone over the eastern United States. Figure 3 shows 500-hPa geopotential heights as analyzed in EDAS. Throughout the 24-h period, it is clear that a

trough is propagating eastward, but flow over east-central Missouri remains relatively weak at 500 hPa. The surface also shows few synoptic-scale disturbances around the St. Louis region. With higher mean sea level pressure to the east, the 1200 UTC 1000-hPa analysis reflects the strong eastern United States high pressure system (Fig. 4). Wind flow around the Missouri region is generally weak from the south to the southwest. There

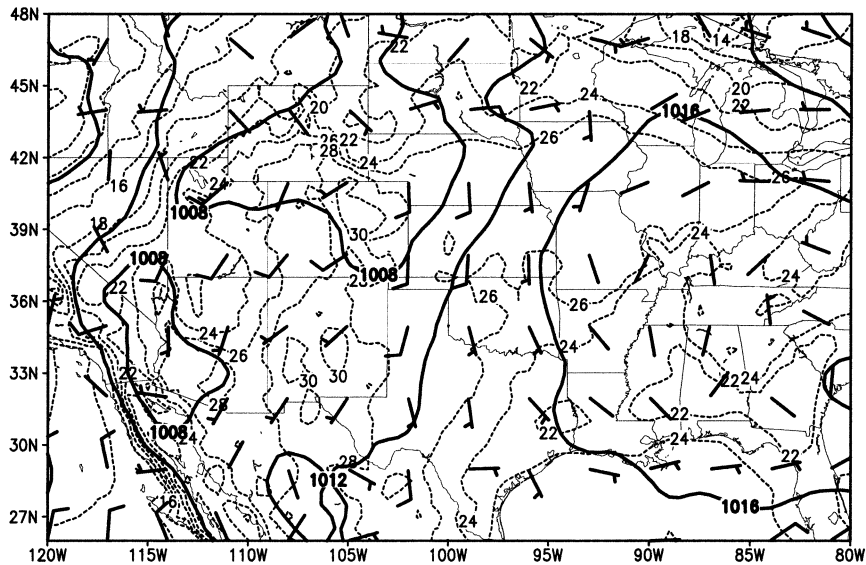


FIG. 4. EDAS 1000-hPa analysis of temperature (dashed contour; interval 2°C) and wind barbs (m s^{-1}) at 1200 UTC 8 Jun 1999. Mean sea level pressure (solid contour; interval 4 hPa) is superimposed on the analysis.

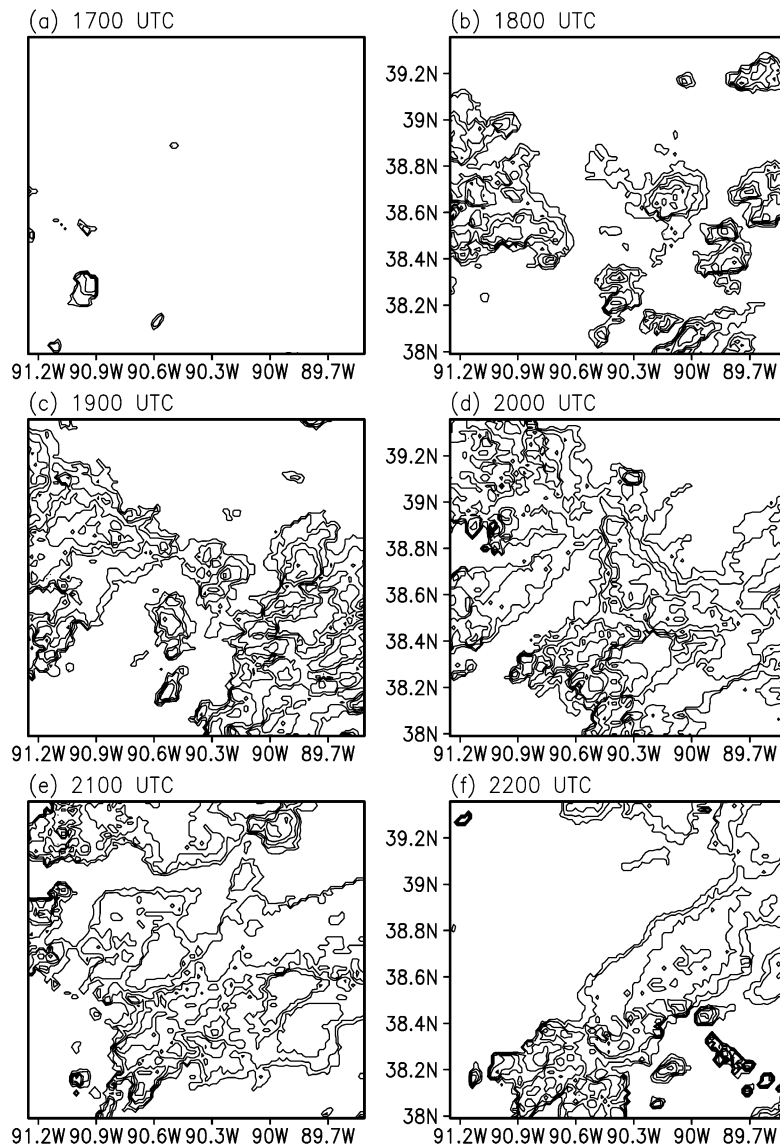


FIG. 5. Composite radar images over St. Louis for (a) 1700 (b) 1800, (c) 1900, (d) 2000, (e) 2100, and (f) 2200 UTC 8 Jun 1999. Contour intervals are provided every 10 dBZ.

is a slight baroclinic zone to the southeast of St. Louis. This aside, no striking synoptic-scale features appear to present obvious thunderstorm-lifting mechanisms around St. Louis, although the environment is favorable for storms because the air is moist and unstable. In the morning of 8 June 1999, a 1200 UTC sounding (figure omitted) from Springfield, Missouri, which is modified to account for the predicted maximum temperature, indicates that the atmosphere contained 1500 J kg^{-1} surface-based convective available potential energy (CAPE).

The storm evolution over St. Louis is visible by radar (Fig. 5). Radar data are derived from archived $2 \text{ km} \times 2 \text{ km}$ National Weather Service composite reflectivity.

Storms began developing around 1645 UTC. By 1700 UTC, a substantial storm formed directly southwest of the city (near 38.3°N and 91°W). Within the next hour, a rather large storm cluster developed just east of downtown St. Louis (near 38.7°N and 90.1°W). Other storms initiated around the peripheries of the domain. The storms southwest of St. Louis broaden and generally move northward. The large storm complex east of downtown, which produced wind damage, moved over the city (near 38.7°N and 90.3°W) by 1900 UTC. Other storms to the west appeared to merge with existing storms over the city by 1930 UTC, bringing heavy precipitation to St. Louis around 2000 UTC. By 2100 UTC, a storm complex moved northward, and an organizing

line of storms, oriented southwest to northeast, began propagating slowly southeastward. The most intense storms quickly dissipated after 2300 UTC. Only light widely scattered showers persisted in the area until 0200 UTC 9 June 1999.

b. Simulated synoptic situation

The control experiment depicts the overall 500-hPa pattern fairly well over the 24-h period, capturing the main features of the ridge and its eastward propagation. General features in the EDAS surface data are reproduced in the RAMS simulations. Although slightly cooler than EDAS, model temperatures are reasonable in the southern and southwestern part of the domain. For the first 17 h of simulation, there is an average model grid-2 bias of -0.973°C . This discrepancy is partially due to a somewhat cold grid-2 initialization (i.e., -0.5°C) and is also due to underpredicted nocturnal clouds in the simulation. Wind vectors are also reproduced fairly well by the model. Both EDAS and RAMS show light wind from the south in the center of the domain.

c. Site comparisons of schemes

A brief comparison of near-surface meteorological fields for urban grid points is carried out between observations, the LEAF-2 urban simulation, and the TEB control simulation (referred to hereinafter as f_{123}). Limited observation sites existed in the St. Louis metropolitan area on 8 June 1999, with only one site located in the city. An objective analysis of RAMS fields (distance-weighted interpolation) yielded comparison data for the stations.

After comparing 2-m temperature and 48-m dewpoint temperature from stations around the St. Louis area with model results, the only station where significant differences between f_{123} and L2 simulations occur is STL. STL is located at Lambert—St. Louis International Airport (38.75°N , 90.37°W), which is the closest observational site to the built-up portion of St. Louis. Because of uncertainties on par with the model–observation differences, similarity theory is not used to reduce the 48-m model dewpoint to 2 m. Figures 6a and 6b illustrate the STL comparison of temperature and dewpoint from 0000 to 1900 UTC, respectively. After 1700 UTC, convection caused substantial differences in model results and observations. Convection was initiated 2 h late in the model.

An obvious cool bias exists the first 14 h of simulation (Fig. 6a). Given the uncertainty in instrumentation, the modeled temperatures are still close to observations. Because convection erupted around 1700 UTC, it is more pertinent to obtain site statistics only up to 1700 UTC. The correlation coefficients for f_{123} and L2 with observations are 0.969 and 0.960, respectively. The bias is -1.016° and -1.820°C for f_{123} and L2, respectively. For dewpoint temperature, correlations are weak with

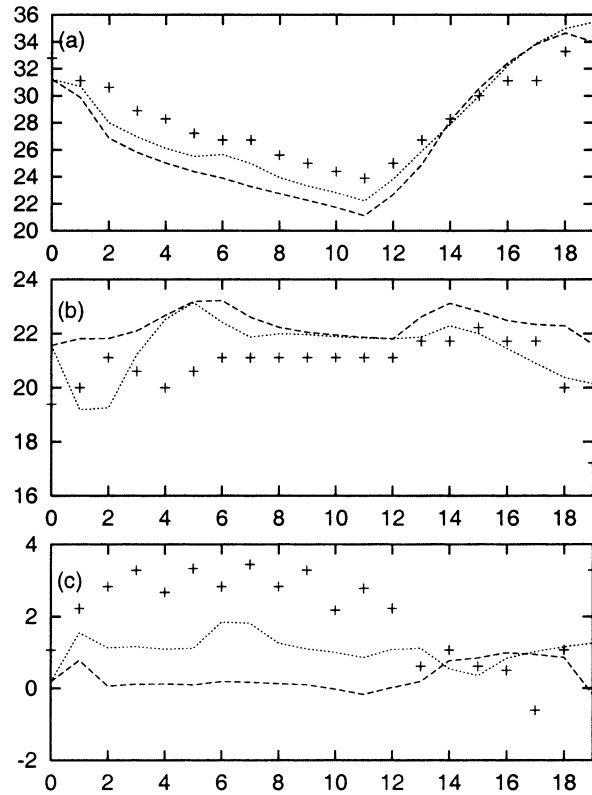


FIG. 6. A comparison of observed (crosses), LEAF-2-simulated (long dashed), and TEB-simulated (dotted) (a) 2-m temperature ($^{\circ}\text{C}$), (b) dewpoint temperature ($^{\circ}\text{C}$), and (c) UHI strength ($^{\circ}\text{C}$) for station STL.

observations, with 0.373 and 0.635 for f_{123} and L2, respectively. A moist bias of 0.588° and 1.314°C holds for f_{123} and L2 dewpoints, respectively.

Clearly, the presence of TEB reduces site biases in temperature and dewpoint. Moreover, the temperature curve's phase of f_{123} with observations is more accurate than L2, especially during the morning hours (i.e., 1100–1600 UTC). This may be attributed to the more realistic simulation of heat storage in TEB, which delays the release of sensible heat to the atmosphere until later in the day. Indeed, the L2 maximum temperature at the site occurs near 1800 UTC, and the f_{123} temperature continues to climb.

There are several reasons for temperature differences between observations and the model. There were few clouds in the simulation, yet scattered clouds were reported throughout the entire observational period. STL data indicated that throughout the night, skies were overcast at heights of 7620 m with scattered low-level clouds. Most of these clouds were left from convection the previous day. During the night clouds likely kept the surface warmer, while during the day scattered cloudiness likely reduced the overall heating. Unresolved clouds may be the reason for overpredicted temperatures between 1600 and 1700 UTC. Additionally,

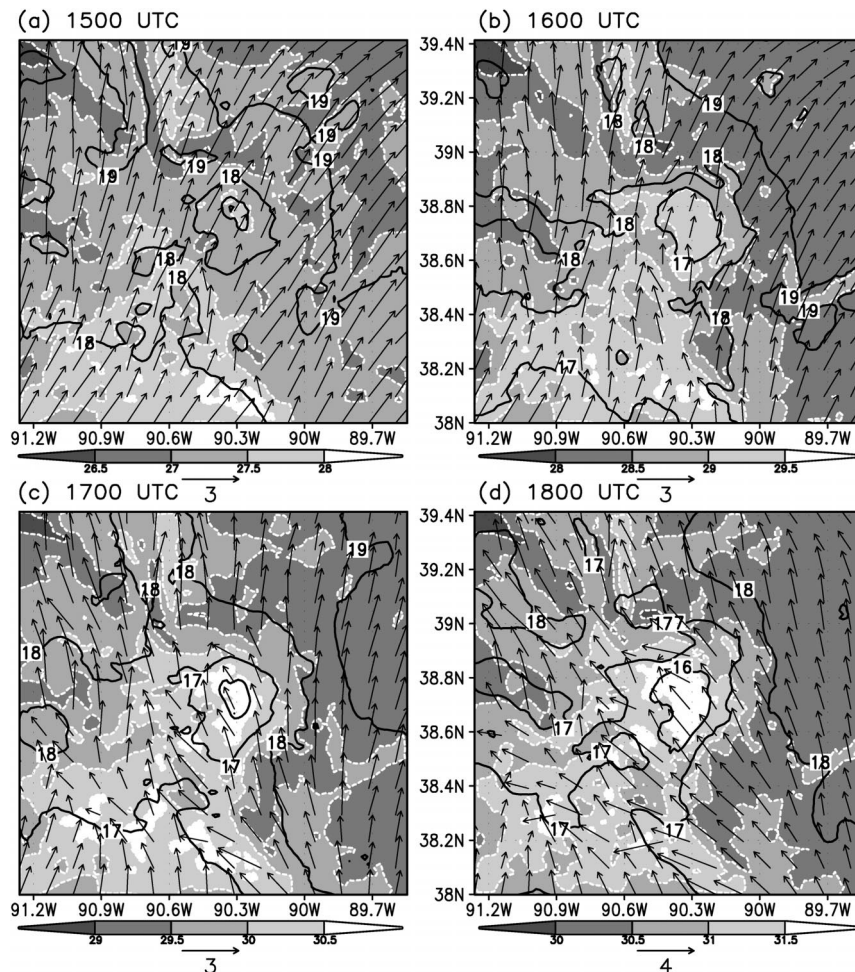


FIG. 7. RAMS evolution of the first model level (48 m) heat island on 8 Jun 1999 with the TEB control simulation. Temperature ($^{\circ}\text{C}$) is shaded, water vapor mixing ratio (g kg^{-1}) is contoured at intervals of 1 g kg^{-1} , and wind (m s^{-1}) vectors are plotted.

temperature and dewpoint were biased through the model initialization.

A rough measure of the UHI is created by a simple difference in 2-m temperature between an urban site and a nearby rural site. A site located on the western edge of the St. Louis suburbs (38.66°N , 90.65°W) is chosen for the rural site. The urban site remains STL. Figure 6c shows the observed, L2-simulated, and f_{123} UHIs for the first 19 h of 8 June 1999. Here, L2 barely produces a nocturnal UHI. Still weaker than observations, f_{123} produces a 1.5°C nocturnal UHI. Perhaps because of variably cloudy conditions, observations are noisy in the midmorning hours. Coinciding with observations, f_{123} produces a slight decline in the UHI in the midmorning hours, whereas L2 immediately creates a UHI in the midmorning.

Obviously, a more reliable comparison lies in the improvement of initial conditions, including soil moisture and temperature, and a refinement of parameters related to boundary layer turbulence. Increased resolution of

the urban surface promises enhanced accuracy. The above method of comparison does not provide a comprehensive validation technique for the TEB. Nevertheless, the point-site comparison reinforces that TEB can perform at least as well as LEAF-2, considering all of the other model discrepancies. Improved and comprehensive validation would include mesonet data.

d. The heat island and convection

Both the LEAF-2 and TEB urban parameterizations produce a UHI during the day of 8 June 1999. Figure 7 shows the evolution of the control simulation heat island from 1500 to 1800 UTC. The f_{123} heat island begins intensifying by 1600 UTC. At 1800 UTC, a heat island of almost 2°C has formed, slightly stronger than the UHI of L2 (figure omitted). At this moment, the average sensible heat flux over the city in f_{123} is about 80 W m^{-2} higher than in L2. Water vapor mixing ratios are substantially lower over the city than in surrounding

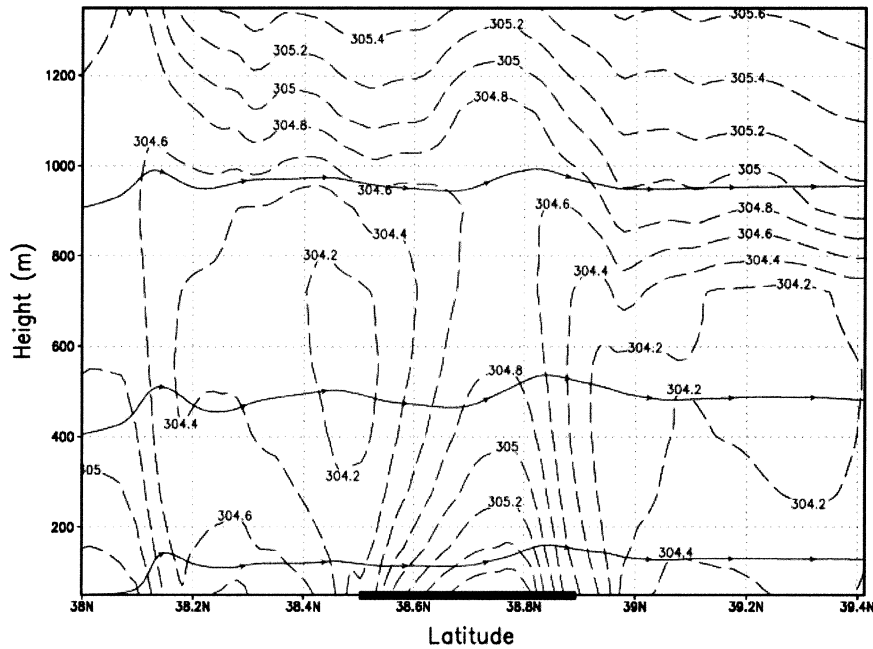


FIG. 8. Vertical cross section (90.3°W) of θ (K) and streamlines at 1800 UTC for the control simulation. St. Louis is located roughly between 38.5° and 38.9°N .

areas for the entire 4-h period. Confluence of the surface wind over and downwind of St. Louis increases throughout the morning. Wind throughout the period becomes more south to southeasterly from boundary layer mixing. In observations, winds are more southwesterly.

Figure 8 shows an 1800 UTC vertical cross section of potential temperature (θ) and streamlines at 90.3°W . Defining the top of the boundary layer to exist at the level of stable static stability (i.e., where θ contours are not vertically aligned), the top of the boundary layer over St. Louis is roughly 300 m higher than rural surroundings. Such boundary layer doming is consistent with heat island studies from METROMEX (e.g., Spangler and Dirks 1974; Hjelmfelt 1982). This enhanced boundary layer denotes the urban boundary layer (UBL). A convective cell forms in the heat island vicinity, with downward motion outside of the UBL and upward motion within the UBL. Subsidence and decreased boundary layer depths are apparent on the edges of the UBL. Another noteworthy aspect is that the UBL is offset by about 0.05°N , demonstrating the downwind advection of the UHI and its convective cell. The results of L2 are qualitatively similar to the results of f_{123} and, therefore, are omitted.

Vigorous cumulus convection forms around 1800 UTC in the simulations. By 1900 UTC, both L2 and the control simulations produce deep, moist and precipitating convection, coinciding with the convergence area in the first model level (48 m). Comparison between radar observations and model output would be appropriate by offsetting the comparison times by about 2 h,

because storms observed by radar were evident at 1700 UTC.

Figure 9 illustrates vertically integrated condensate and total precipitation for the first 6 h of convective storms in the control simulation. A storm initiates downwind of St. Louis by 2000 UTC. In L2, a storm initiates in this same location 1 h earlier. Incidentally, a radar-detected storm forms at 1800 UTC on the eastern edge of downtown St. Louis. It is not clear why a storm was observed in this particular location, nor can urban effects be proven to have caused this storm. High-density surface data are not available to confirm this possibility. The radar-detected storm did form in the hypothetical downwind convergence zone of St. Louis. (Surface winds were more westerly in observations than in the model.) Nevertheless, downwind convective development in the model is consistent with METROMEX results. Throughout the period the control simulation does an inadequate job of resolving storms that were observed near the eastern boundary in grid 3. For modeled storms south and west of the city, there is a general southeastward movement of the storms. This southeastward progression is consistent with radar data. Overall, the similarity between radar data and the control simulation is not bad, given the difficulty in accurately predicting the spatial and temporal distribution of isolated cumulonimbi. Because modeled storms initiated downwind of the city, precipitation totals of about 80 mm fell downwind of the city in the control simulation.

After 6 h, storms around the region dissipated in the observations, and all of the model simulations continued

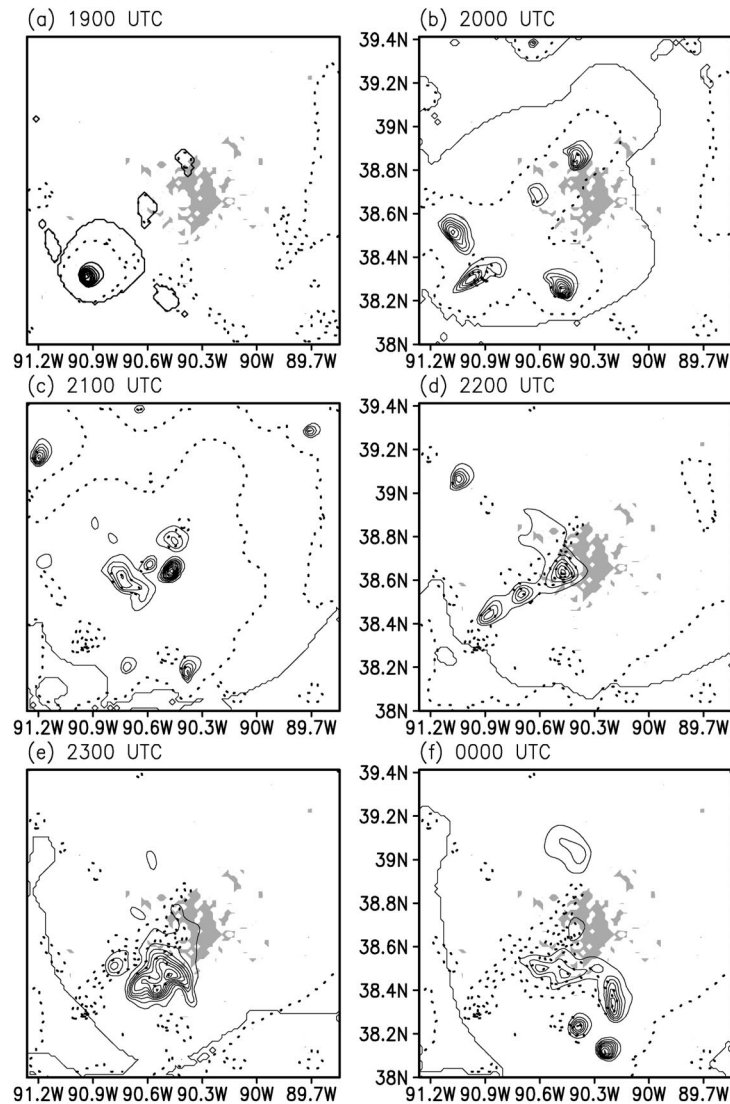


FIG. 9. Control-experiment hourly vertically integrated condensate (solid contours, with 5-mm intervals) and total precipitation (dashed contours, with 40-mm intervals). Dominant patch urban class 30 is shaded.

producing convection around some domain peripheries. Because the model results correspond well to observations for the first 6 h with the timing offset, comparisons are made only up to the sixth storm hour. Therefore, all sensitivity simulations are analyzed through 0000 UTC 9 June 1999.

4. Simulation of urban versus nonurban effects

Factor separation techniques help determine how topography, urban heat and radiative fluxes, urban momentum flux, and their interactions influence the outcome of the control simulation. Atmospheric phenomena not explained through variations in these parameters remain in the base simulation (i.e., f_0). The base simulation removes the urban land and topography. Tables

4 and 5 explain the experiment symbols used hereafter. Many of the model analyses are based at 1800 UTC, because this time marks the height of the daytime UHI and it is when convective clouds begin forming.

Figure 10 displays total precipitation from the 6-h period of convection for experiment f_0 . The vast majority of storms are located over areas of significant precipitation totals. Except for the storms in the southwestern sector of the domain, the remaining hourly storms are placed at distinct locations from one another. The intense stages of the storms are short lived and move little in the horizontal. An important point illustrated in Fig. 10 is the absence of accumulated precipitation downwind of St. Louis. Nonurban land use variation is certainly a candidate for forcing the initial storms in this experiment.

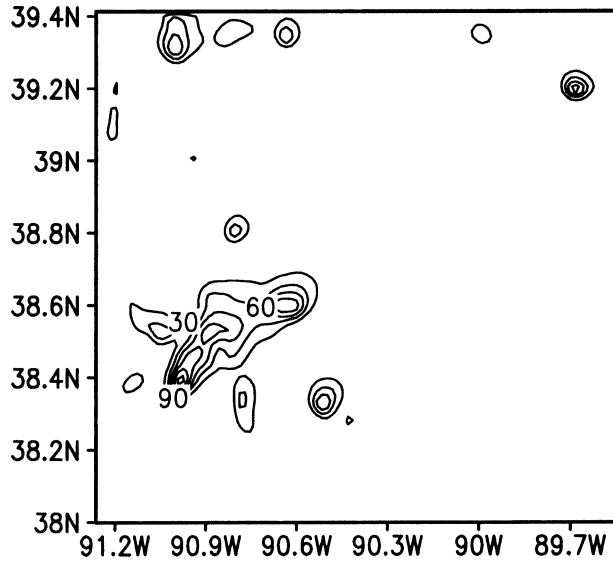


FIG. 10. Total precipitation (mm) for f_0 at 0000 UTC 9 Jun 1999. Contour interval is 30 mm.

a. Contribution by topography

In grid 3, the largest topography variations occur northwest (north of 39°N and west of 90.6°W) and southwest (south of 38.5°N and west of 90.4°W) of St. Louis. As a result, these are the areas where the largest atmospheric differences between f_0 and f_2 are expected. Recall that f_2 replaces all urban land use by rural vegetation and associated LEAF-2 biophysical parameters, but retains high-resolution topography.

Figure 11a provides the 48-m 1800 UTC difference

field corresponding to \hat{f}_2 for temperature, water vapor mixing ratio, and wind vectors. Northeast of St. Louis, topographic features promote cooler air than the smoothed topography, coinciding with a strong response in surface wind. Westerly wind is enhanced about 1 m s⁻¹ in this region. Larger variations in temperature result northwest of St. Louis where larger variations in topography along the Mississippi and Illinois Rivers reside. Associated with the Ozark foothills southwest of town are areas of warmer temperature. Relative to the simulation with smoothed topography, warmer temperatures in f_2 occur at lower elevations. On the other hand, potential temperature (not shown) increases with elevation. Wind is directed up and out of valleys toward the southwest. Such wind flow appears to be consistent with slope–valley circulations described by Johnson and Toth (1982). It must also be brought to attention that the nonlinear interaction of natural vegetation variability and topography may also influence wind.

Surface divergence and surface-derived CAPE variations of \hat{f}_2 at 1800 UTC are shown in Fig. 11b. The greatest convergence areas occur in the foothills of the Ozarks. These convergence zones are associated with larger perturbations in CAPE. Assuming that the lapse rate is approximately uniform in the southwestern sector of the domain, the increase in surface instability is primarily caused by enhanced moisture convergence. Evidently, these variations near the Ozark foothills are sufficient to initiate storms.

Figure 12 shows the first 3 h (1900–2100 UTC) of storms (vertically integrated condensate) and the total precipitation at 0000 UTC. (Convective initiation is seen in Figs. 19a–c.) The development of a storm at 1900

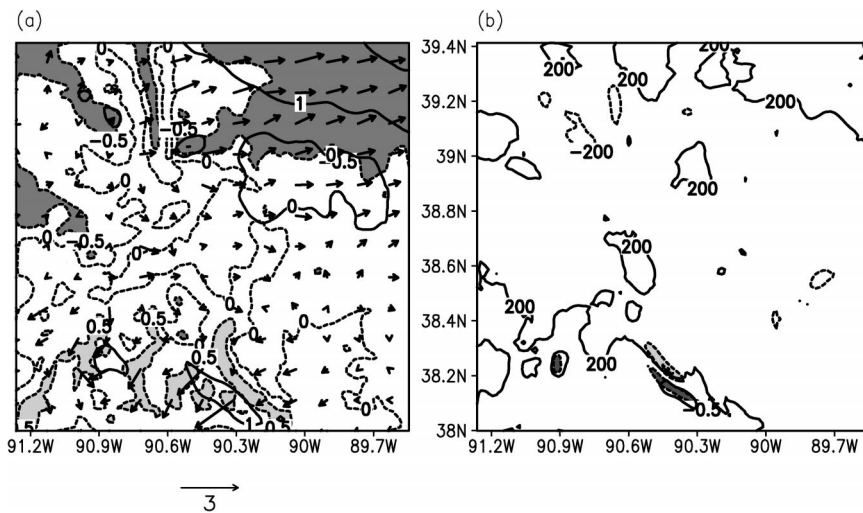


FIG. 11. (a) Difference field at the 1800 UTC first model level (48 m) showing temperature (dashed contour at every 0.5°C; dark and light shading when temperatures are below -0.5° and above 0.5°C, respectively), water vapor mixing ratio (solid contour at every 1 g kg⁻¹), and winds (m s⁻¹ reference vector at bottom of panel) in \hat{f}_2 . (b) Corresponding difference field showing 48-m divergence [dashed contour every 0.5 (1000 s⁻¹); dark and light shading when divergence is below -0.5 and above 0.5 (1000 s⁻¹), respectively] and surface-derived CAPE (solid contour: J kg⁻¹).

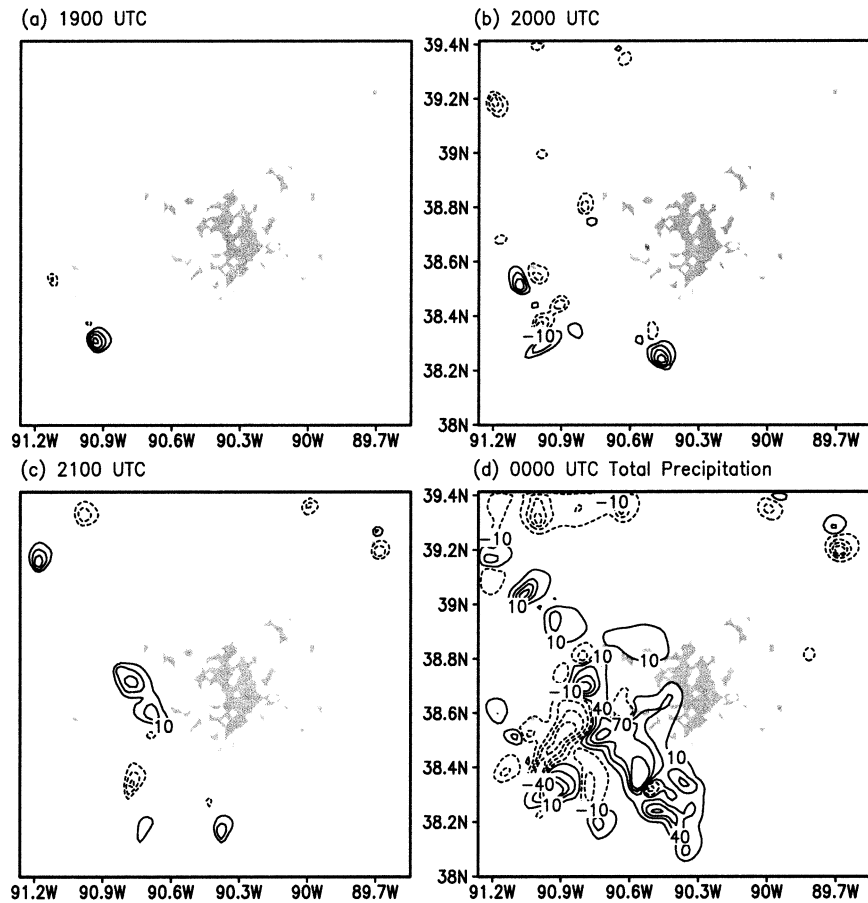


FIG. 12. Difference fields for \hat{f}_2 of vertically integrated condensate at (a) 1900, (b) 2000, and (c) 2100 UTC 8 Jun 1999 (contour interval 10 mm, positive solid, negative dashed), and (d) total precipitation at 0000 UTC 9 Jun 1999 (contoured every 30 mm). Urban class 30 is shaded to indicate position of St. Louis.

UTC, with 40 mm of vertically integrated condensate, is associated with the convergence zone located furthest west at 1800 UTC. By 0000 UTC, the area-weighted average total precipitation for f_2 was 9.22 mm, whereas the same calculation from f_0 yielded 6.78 mm. With more storms initiated, more precipitation falls in f_2 . In both cases, most of the precipitation fell in the southwestern sector of the domain, with topography promoting enhanced precipitation. In comparison with the control simulation, no substantial increase in total precipitation is seen downwind of St. Louis, except for a slight area exceeding 10 mm on the northwestern side of St. Louis. The origin of this precipitation anomaly is the development of a storm caused by the outflow of other storms.

A variety of ambiguities remain since METROMEX regarding the function of topography on St. Louis regional rainfall anomalies. METROMEX showed a “minor” rainfall maximum in the Ozark foothills region (Changnon 1981). In this individual case study simulation, these foothills had a meaningful impact on storm development. Other topographic features highlighted during METROMEX, such as the southeastern bluffs

along the Mississippi River and the “bottomlands” north of town, play little role in initiation in the current simulations. In these areas, convergence driven by topographic features is not comparable with convergence due to other factors, especially the yet-to-be-discussed UHI-induced convergence. A number of distinct simulations are needed before a complete knowledge of the impacts of topography on storms can be solidified.

b. Contribution by urban heat and radiative fluxes

Experiment f_1 adopts a rural formulation of momentum flux and smoothed topography, but adopts an urban energy balance. The differences between f_1 and f_0 demonstrate contributions to convective activity solely by the UHI. The UHI is actually intimately related to the other factors, which will be shown later. To first order, the UHI is due to the gradients in energy balance terms across the urban–rural boundaries, as captured in f_1 .

Figure 13a shows the \hat{f}_1 difference field of temperature, water vapor mixing ratio, and wind vectors at 1800 UTC. Urban turbulent heat flux and upward radiation

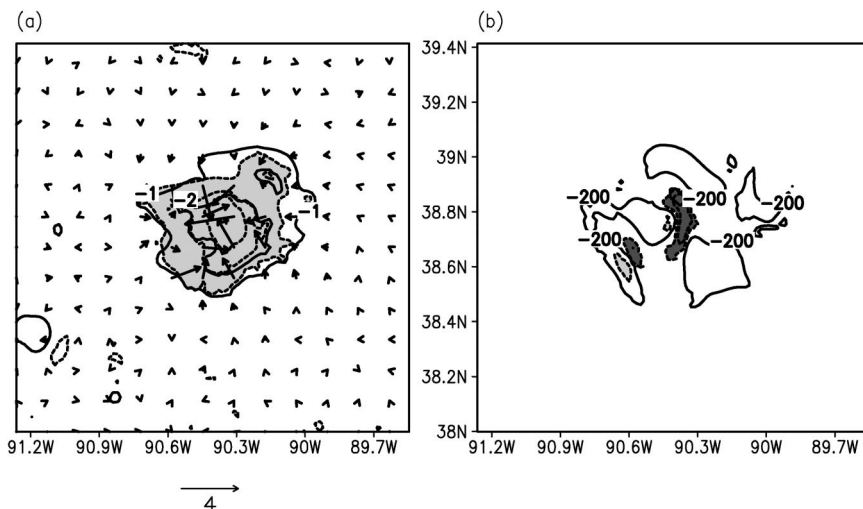


FIG. 13. Same as in Fig. 11, but for \hat{f}_1 .

promote a substantial heat island of nearly 2°C. There is also a second UHI to the northeast of St. Louis, which is located over the area of Alton, Illinois. The UHI wind flow is directed inward, consistent with a full UHI circulation. The boundary layer convection (not shown) is enhanced within the heat island. Temperature and wind fields do not greatly differ in nonurban areas. In contrast, the maximum temperature difference situated north (downwind) of St. Louis is associated with the strong gradient in land use. The center of the UHI is advected downwind of the center of St. Louis. In addition, the water vapor mixing ratio is substantially lower within the heat island. A deficit exceeding 2 g kg⁻¹ is apparent. The water vapor mixing ratio is much lower within the UHI because of the relatively lower latent heat flux.

Surface-derived CAPE and surface-divergence (Fig. 13b) modifications become obvious with the inspection of \hat{f}_1 . Even with enhanced surface temperature, the urban area generally decreases CAPE. The primary culprit is the reduction in water vapor over the city. CAPE is further reduced in areas of positive divergence, due to subsidence stabilization and also divergence of water vapor. An exception to the urban CAPE reductions is in the center of the UHI, where surface convergence is rather large ($< -1.5 \times 10^{-3} \text{ s}^{-1}$). Here, water vapor convergence is large. By 1800 UTC, enough water vapor has converged in the UHI center to increase the CAPE by over 100 J kg⁻¹. Collocated with the UHI convergence is rising air in the UBL. Compensating subsidence takes place around the UHI, especially to the west-southwest and east-northeast of the strong convergence center. Therefore, areas of surface divergence exist in these locations. One other convergence/divergence couplet appears in Fig. 13b, around 38.6°N and 90.6°W. In relation to the land use around St. Louis (Fig. 1), this couplet is located along the southwestern suburban frontier of St. Louis. In this area, a broad area of deciduous broadleaf forest sits next to residential areas, and the

gradient in Bowen ratio is coincidentally large. Such strong couplets are not as apparent in other suburban frontiers, because the land use and subsequent Bowen ratio variations are smaller in those areas. In general, large variations in surface temperature promote a considerable wind field response.

Figure 14 demonstrates the differences in storm initiation and 6-h (0000 UTC 9 June) precipitation difference totals corresponding to \hat{f}_1 . By 1900 UTC, the UHI-based convergence initiates a thunderstorm on the leeward edge of St. Louis. Like the control simulation, it is clear that the UHI convergence area creates a storm, but now the downwind storm develops 1-h earlier. By 2000 UTC, a storm forms over the convergence area near the southwestern suburban edge.

Outflow from the urban-based storms generates more vigorous convection than f_0 through 0000 UTC 9 June. The area-averaged precipitation at 0000 UTC is 8.32 and 6.78 mm for f_1 and f_0 , respectively. The UHI notably increases precipitation totals downwind of St. Louis. Areas of increased precipitation extend from a maximum on the edge of St. Louis to another maximum further downwind, with total precipitation exceeding 70 mm within both maxima. This total precipitation enhancement is greater than in the control simulation. In future work, performing an ensemble of simulations will elucidate surface boundary condition impacts on storm evolution and total precipitation.

These results agree with previous modeling and observational studies in that the UHI plays a central part in initiating storms that are apparently enhanced by the urban surface. In fact, the 2D modeling results of Thielen et al. (2000) indicate that sensible heat flux variations, due to the urban surface, provide the largest impact upon convection. Observational case studies of Bornstein and Lin (2000) are consistent with the results in this study, but their preconvective surface convergence values were much smaller (with maximum con-

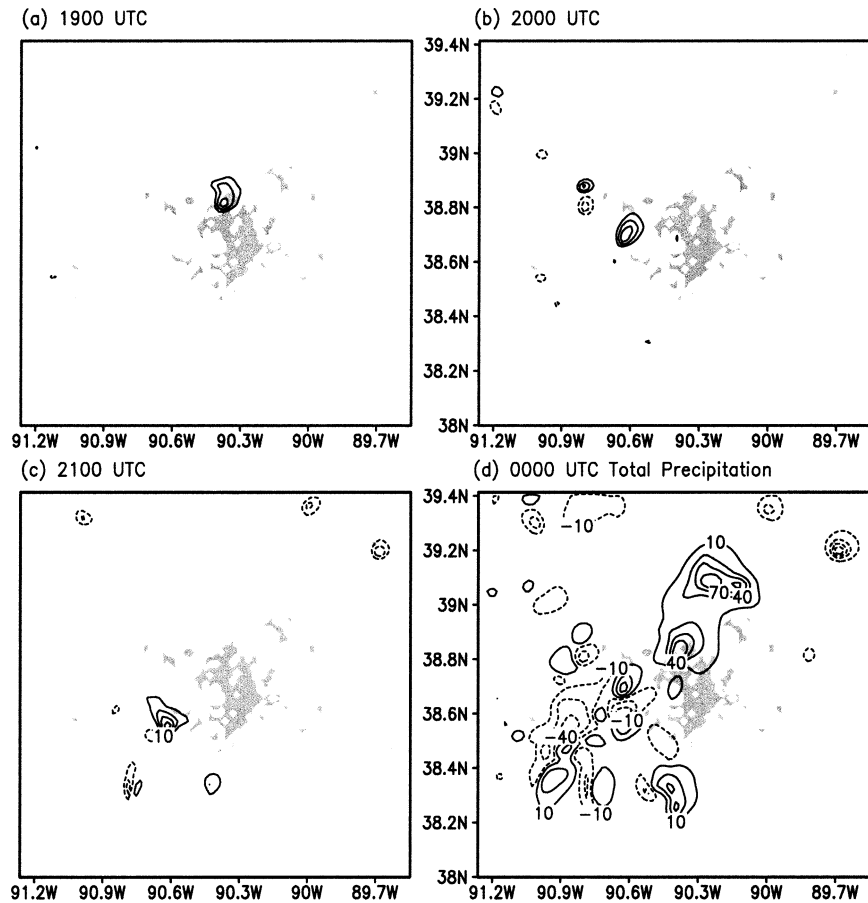


FIG. 14. Same as in Fig. 12, but for \hat{f}_1 .

vergence on the order of $1 \times 10^{-4} \text{ s}^{-1}$). The position of the UHI-induced boundary layer updraft cell and resulting thunderstorm qualitatively agrees with Baik and Kim (2001), in that the basic-state wind places convection downwind of the heating source. In summary, the UHI convergence occurs downwind of the city. As a result, deep, moist convection initiates on the leeward side of the city. Furthermore, vigorous convective initiation downwind of the UHI leads to increased total precipitation downwind of the city.

c. Contribution by urban momentum flux

The addition of urban-simulated momentum flux to the configuration of f_0 is the focus of experiment f_3 . Figure 15a illustrates difference fields of temperature, vapor, and winds corresponding to \hat{f}_3 at the 48-m level. Temperature differences are not significant, but the water vapor mixing ratio is slightly higher over the city with respect to rural values just outside of St. Louis. Wind differences compose the most marked feature. In the vicinity of the city, winds are directed toward the south-southeast, with an average magnitude on the order of 1 m s^{-1} . Clearly, the effect of momentum drag by

the city is exemplified, because wind decelerates with respect to the rural background wind. In small, sparse urban centers northeast of the city, there are various wind anomalies due to modified momentum flux.

Wind modifications shown in \hat{f}_3 change divergence patterns at the surface. Urban-calculated momentum flux forces surface convergence, along with slightly higher CAPE, on the southern (windward) edges of the city at 1800 UTC (Fig. 15b). Surface divergence, associated with lower CAPE, is found on the leeward side of the city. The magnitude of divergence is an order of magnitude less than that seen in either \hat{f}_1 or \hat{f}_2 . The urban-produced convergence in f_3 is positioned on the opposite side of the city from the UHI-produced convergence. In fact, surface divergence replaces the area of convergence in simulation f_1 . CAPE differences are mostly due to subsidence-induced warm air, located aloft within the area of descending air (figure omitted). Vertical motion is positive (approximately 2 cm s^{-1}) on the windward side of the city, with the city located roughly between 38.5° and 38.9°N . Compensating downward motion of approximately -2 cm s^{-1} occurs on the leeward side of the city.

As it turns out, storms are not initiated over St. Louis

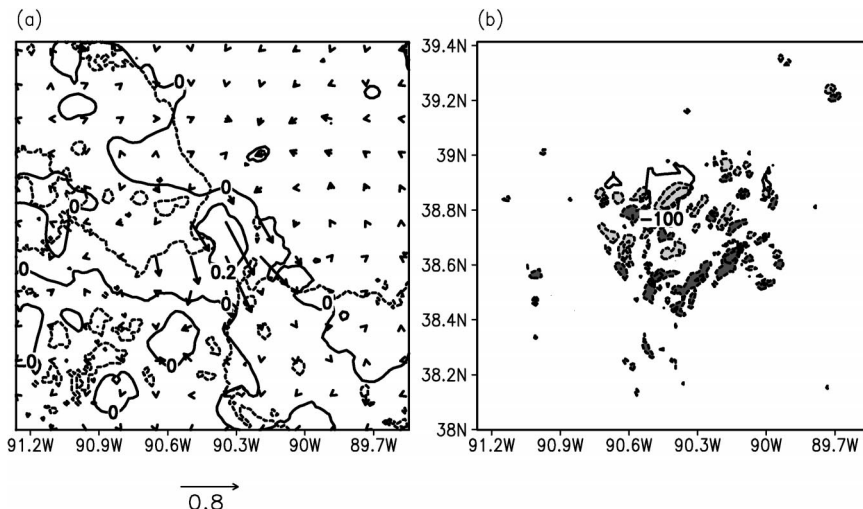


FIG. 15. Same as in Fig. 11, but for f_3 . Now water vapor mixing ratio is contoured at 0.2 g kg^{-1} and surface divergence is shaded lightly and darkly for values above 0.05 and below -0.05 (1000 s^{-1}), respectively, and contoured at increments of 0.05 (1000 s^{-1}). CAPE is contoured every 100 J kg^{-1} .

when only momentum flux representative of St. Louis is used (figure not shown). The convective environment evolves similarly to f_0 . However, because meteorological fields vary slightly, after 3 h into the convective episode, the evolution differs a little from f_0 . These anomalies lead to slight modifications in the total rainfall patterns seen in Fig. 10. The results do not infer a major impact on convection by the roughness of an urban surface alone, at least under the meteorological conditions of moderate surface winds (5 m s^{-1}) and an unstable surface layer.

Thielen et al. (2000) show that roughness alone impacts storm initiation. Moreover, Thielen et al. found that increased roughness length enhances storms. Their study was limited to 2D, excluding possible airflow around the city.

It is worthwhile to consider the role that urban momentum flux plays in the strength of the heat island. Can urban fluxes be truly separated from one another to objectively discern their physical contributions to the atmosphere? Also, it was previously demonstrated that storms downwind of St. Louis develop 1 h earlier in f_1 than in the control simulation. Can this offset be explained solely by the linear superposition of divergence from f_1 and f_3 ? A similar storm-timing offset is found between the control study and a simulation including topography and the UHI, but simulates rural momentum flux (i.e., f_{12}). For brevity, the difference between f_{12} and f_{123} is defined as roughness variation (RV) hereinafter.

Figure 16a illustrates the 1800 UTC difference fields of temperature, water vapor, and winds at 48 m for RV. Replacing urban momentum flux by rurally formulated momentum flux increases the temperature (and the UHI) downwind of the city but reduces the temperature on

the windward side of the city. Overall, the magnitude of the wind is greater in f_{12} , because the eddy drag on flow decreases and the heat island circulation strengthens. Water vapor mixing ratio increases in this vicinity.

The 1800 UTC surface divergence and CAPE differences in RV are shown in Fig. 16b. Where surface convergence is strongest, the largest increases in CAPE are produced. This enhancement in CAPE is primarily the result of water vapor convergence. Clearly, surface convergence in f_{12} is larger than divergence caused by urban momentum flux downwind of the city, by almost 1 order of magnitude. This means some feedbacks have occurred. The explanation for this increased convergence is that thermal perturbations predominantly drive it. As a result of the increased downwind UHI for RV, a downwind storm initiates 1 h earlier than in the control simulation.

Why does smaller-magnitude surface momentum flux modify the strength of the heat island downwind of the city? Using the sensible heat flux formulation of TEB and meteorological output from the simulations, the contribution to increased sensible heat flux (H) by increased wind speed and relevant thermodynamic variables (i.e., water vapor content and temperature) may be determined. Differences in sensible heat flux are obtained from experiments f_{12} and f_{123} , in which representative urban values are used within downtown St. Louis. Contributions to differences in H are determined for changes in wind speed, changes in the thermodynamic variables, and the nonlinear interactions of both wind and thermodynamic variables. The contributions are expressed as percentages of the total sensible heat flux difference.

Figure 17b illustrates the computed difference fractions at hourly intervals between 1400 and 1800 UTC. After 1800 UTC, differences in convection disrupt use-

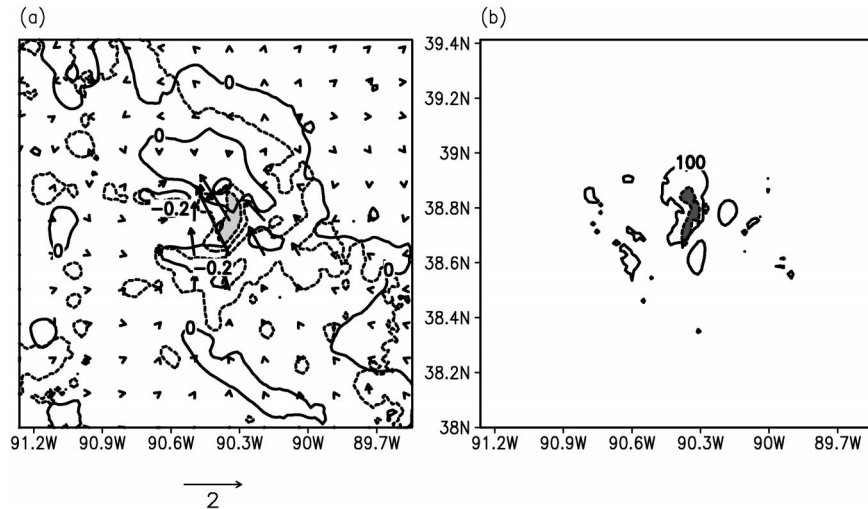


FIG. 16. Same as in Fig. 12, but for differences between f_{12} and f_{123} . Also, water vapor mixing ratio is now contoured at 0.2 g kg^{-1} and temperature is shaded lightly and darkly for values above 0.2° and below -0.2°C , respectively. CAPE is contoured every 100 J kg^{-1} .

ful comparison. Before 1400 UTC, sensible heat flux differences are much smaller, and they are not essential to the development of the daytime heat island (Fig. 17a). The nocturnal heat island is largely produced by the anthropogenic heat sources, which are equivalent in both experiments. The wind speed increases in f_{12} are most responsible for increases in sensible heat, accounting for 1.06% of the changes in H in the mean. The mean percentage change caused by thermodynamic changes is 0.05. Nevertheless, thermodynamic modifications become increasingly important throughout the period, and eventually contribute to a rise in the sensible heat flux. This is because the surface layer of f_{12} becomes increasingly more unstable than the surface layer of f_{123} . Nonlinear interactions always provide a small negative contribution to the total change in H . Nonlinear interactions account for an average of about -0.04 of the change in H .

In summary, it is apparent that the sensible heat flux increases and the strengthened UHI at 48 m are caused by the increased wind strength over the city. These results seem to differ from those of Morris et al. (2001) and others, in that the UHI actually increases with wind speed rather than diminishes with wind speed. However, as Fig. 18 indicates, even though air temperature increases at 48 m, the temperature at rooftop level (in the model's surface layer) decreases significantly in f_{12} . UHI measurements from the literature, taken at typical instrument-height levels, are consistent with the current results at rooftop level. On the upwind side of St. Louis, the net result of increased winds reduces the temperature at both 48 m and rooftop height (Fig. 16a). It is important to consider that this experiment relates exclusively to wind changes directly over the city, rather than broadscale ambient wind changes. Furthermore, urban parameters are changed in an ad hoc manner in that

some urban parameters are neglected, whereas observations are usually taken with all urban properties rigidly present.

It is questionable whether the factors of heat flux and momentum flux may be separated in reality. To separate one factor from another, the feedbacks between factors must be taken into consideration. For example, momentum flux generated by an urban area decreases the strength of the UHI, thus, decreasing the UHI factor's influence on storm development. On the other hand, assuming a UHI is present with surface flow, if we wish to only determine the effect of an urban barrier on flow, the study is flawed if the UHI-driven wind is not considered. In addition, a significant component of the total urban wind is neglected. Further behavior of feedbacks, or interactions, may be better understood by developing difference fields that represent interaction contributions.

d. Interactions between factors

Although it is inherently difficult to isolate individual contributions to urban-induced thunderstorms in observations, it is instructive to examine different interactions of sensitivity components. Figure 19 (1800 UTC) shows that such interactions lead to a substantial amount of variability in temperature, water vapor, and wind. Interactions between topography and urban energy balance fluxes lead (i.e., experiment \hat{f}_{12}) to significant temperature variations on the northern edge of St. Louis, as seen in Fig. 19a. Here, temperature ranges about 0.3°C . In Fig. 19b, temperature varies little, indicating that the interaction between urban momentum flux and topography is small. Figure 19c shows a temperature spread across the domain of 0.5°C . These variations are the result of interactions between the UHI and the urban

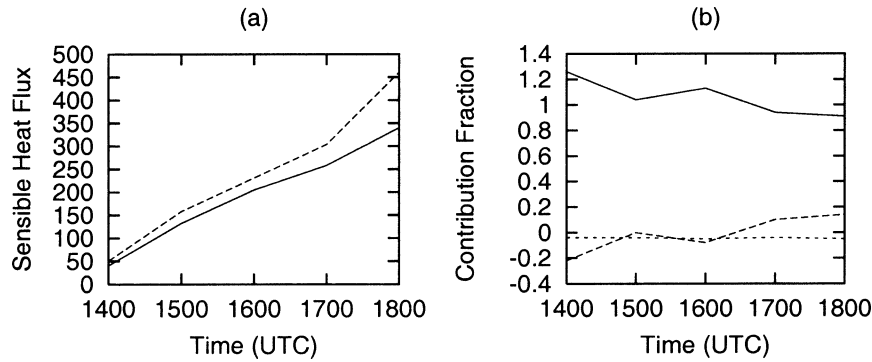


FIG. 17. (a) Sensible heat flux ($W m^{-2}$) calculated at a point in the center of the city, for experiments f_{12} (dashed) and f_{123} (solid). (b) The contribution ratio of wind speed changes (solid), thermodynamic changes (long dashed), and nonlinear interaction changes (short dashed) to total sensible heat flux differences. The differences are with respect to f_{12} and f_{123} .

momentum flux. The existence of such interactions was established earlier. Here, the feedbacks between the UHI and urban momentum flux create cooling on the northern portion of the city and warming on the southeastern section. This is consistent with increased momentum flux and subsequently decreased sensible heat flux. In Fig. 19d, the temperature variations resulting from the interactions of all three factors are plotted. A slight cooling results on the eastern section of the city. Overall, factor f_1 dominates the pattern of temperature fields in f_{123} with a UHI magnitude of about $2^{\circ}C$.

Also plotted in Fig. 19 are variations of the water vapor mixing ratio. Water vapor exemplifies the largest variations in Fig. 19a. Although the UHI alone decreases water vapor relative to the surrounding environment, the topographic configuration around St. Louis helps alleviate this deficit. Latent heat flux increases by over $20 W m^{-2}$ over the city, but decreases by over $30 W m^{-2}$ immediately north of the city. Figure 19c shows water vapor increases of about $0.2-0.4 g kg^{-1}$ on the outskirts of the city. A slight decrease occurs in the center of the city, coinciding with cooler air. Surface

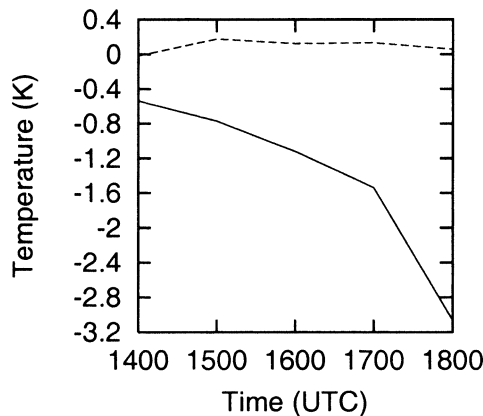


FIG. 18. The 48-m temperature (K) difference (dashed) and surface temperature (K) difference (solid) between f_{12} and f_{123} at the same urban site as in Fig. 18.

divergence patterns, resulting from feedbacks between factors, govern most of the variability in water vapor. Water vapor variations from interactions of momentum flux and topography, and interactions of all three factors prove to be insignificant (Figs. 19b and 19d).

Wind flow, resulting from the interactions, is also plotted in Fig. 19. The surface flow responds slightly to the temperature perturbations shown in the upper left-hand panel, although the magnitude of wind is one-third of that from the flux interactions of Fig. 19c. Wind speed decreases by over $2 m s^{-1}$ in the region of decreased temperature. Such decreases in wind speed explain the sharp drop in latent heat flux and decreases in sensible heat flux of $130 W m^{-2}$ (centered at $38.85^{\circ}N$ and $90.35^{\circ}W$). Feedbacks between topography and the UHI are caused by changes in surface fluxes. These changes in fluxes ultimately feed back to the atmosphere, thus, further changing the wind and surface fluxes. Evolution of these interactions suggests that the higher elevations, with respect to the surrounding river valleys, of northern and western St. Louis drive surface flow up the terrain. In addition, the UHI circulation is superimposed upon this flow. Together, these flows enhance sensible heat flux. Thermodynamical feedbacks drive an additional nonlinear component of the wind, as seen in Fig. 19a. Wind most significantly responds to temperature perturbations produced by the interaction of urban momentum flux and the UHI (Fig. 19c). Because the increased roughness of the city limits the strength of the UHI, confluence of the wind in the UBL is decreased. Recall that the UBL is located on the leeward edge of the city and the UBL is associated with the rising branch of the UHI circulation. Evidently the interactions between urban momentum flux and UHI dampen this circulation, directing flow out of the UBL relative to the current scenario. As expected, the surface wind response is trivial in the right-hand panels, except for some minor response near the city when all three factors interact. The wind flow response largely coincides with gradients in temperature resulting from flux interactions.

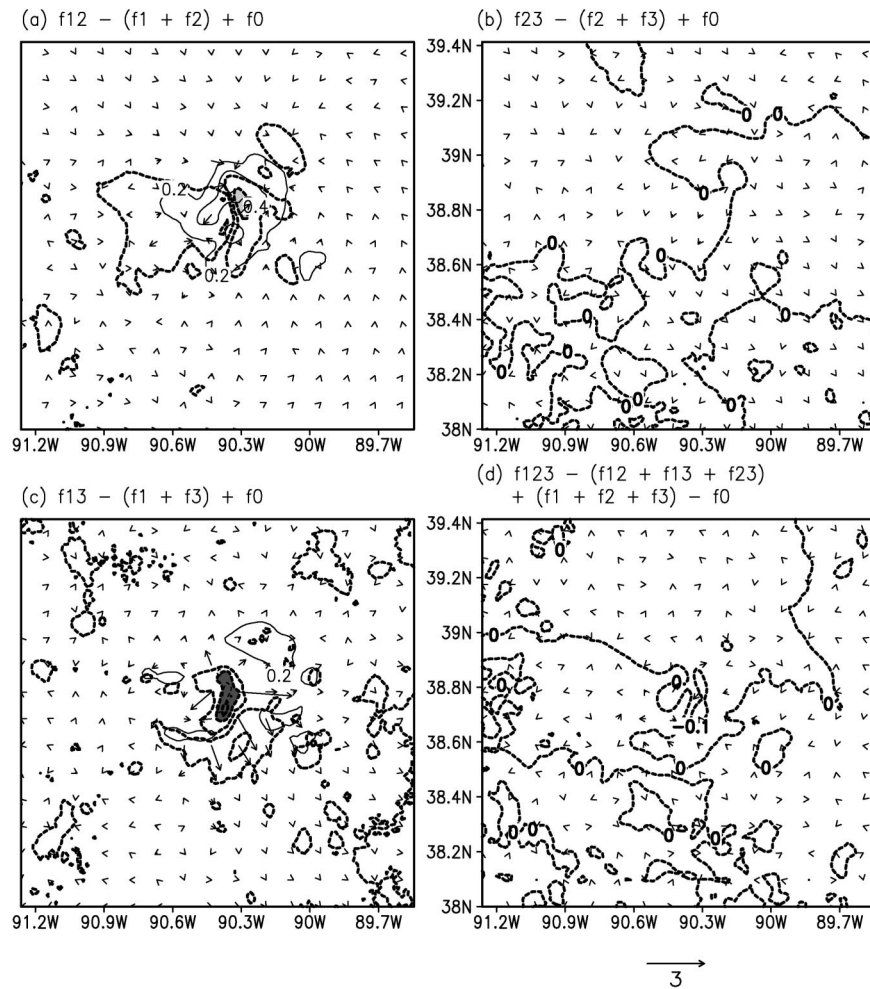


FIG. 19. The 48-m temperature (dashed contour every 0.1°C ; shaded darkly and lightly when below -0.2° and above 0.2°C , respectively), winds (m s^{-1}), and water vapor mixing ratio (solid contour every 0.2 g kg^{-1}) due to (a) \hat{f}_{12} , (b) \hat{f}_{23} , (c) \hat{f}_{13} , and (d) \hat{f}_{123} at 1800 UTC.

Figure 20 shows surface divergence and surface-derived CAPE for the factor combinations alluded to in Fig. 19. The synergy of the UHI and topography leads to a couplet of divergence and convergence along a sharp temperature gradient. The extra divergence downwind of the city helps reduce the early initiation of storms. Over the areas of strongest convergence, CAPE increases by about 300 J kg^{-1} . No consequential changes in surface divergence result in Fig. 20b, consistent with the wind field. Figure 20c demonstrates that the interaction of the UHI and urban momentum flux increases divergence downwind of the city to a magnitude that rivals the convergence resulting from the UHI alone. A small convergence–divergence couplet forms from the thermal perturbations of all three factors (Fig. 20d). Here, CAPE slightly decreases as well (up to about 150 J kg^{-1}), particularly where there is surface divergence.

As a result of convergence patterns due to factor in-

teractions, convective initiation is greatly affected (Fig. 21). Figure 21d is the only panel that indicates an increase in precipitation, revealing that the interactions of all three factors act to enhance storm initiation downwind of St. Louis. The increase in vertically integrated condensate is about 20 mm. This storm enhancement is a result of the gradient in temperature and resulting surface convergence. As Fig. 21b demonstrates, just as in experiments only including topographic or urban momentum flux factors, their interactions do not promote convection around the city at 1900 UTC. Figure 21a provides the storm development from the interactions of topography and UHI. The surface divergence downwind of the city is actually strong enough to decrease the magnitude of the initial downwind storm, even in the presence of greater water vapor. In Fig. 21c, the reduction of the downwind storm is substantial. Indeed, the interaction of the urban momentum flux and UHI slow storm development. The decreased convergence,

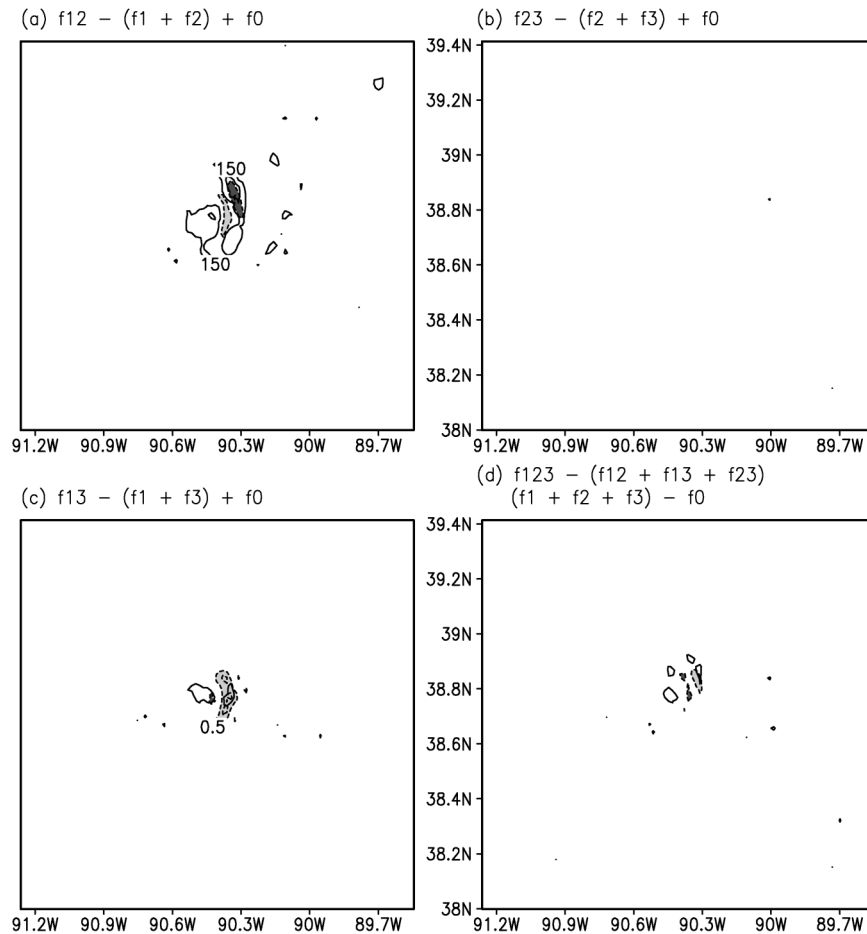


FIG. 20. The 48-m divergence [dashed contours at increments of 0.5 (1000 s^{-1}); shaded darkly and lightly when below -0.5 and above 0.5 (1000 s^{-1}), respectively] and surface-derived CAPE (solid contour every 150 J kg^{-1}) for (a) \hat{f}_{12} , (b) \hat{f}_{23} , (c) \hat{f}_{13} , and (d) \hat{f}_{123} at 1800 UTC.

due to the reduced UHI, is nearly enough to completely deplete the storm that formed because of differences represented by \hat{f}_1 .

Interactions between these factors greatly influence total precipitation patterns. In all panels of Fig. 22, the 0000 UTC total precipitation varies considerably in the southwestern sector of the domain from chaotic storm evolution. Interactions between topography and the UHI tend to reduce the UHI-impacted rainfall maximum downwind of St. Louis (Fig. 22a). This reduction is further seen in the UHI and urban momentum flux interactions (Fig. 22c). These interactions reduce the strength of initialized convection, thus, reducing the total precipitation enhancement on the northern edge of St. Louis. Interactions between all three sensitivity factors accentuate the precipitation totals farther downwind of St. Louis (Fig. 22d). The interactions of either urban momentum flux or topography with the UHI cancel the rainfall anomaly created by the UHI alone or the interactions of all three factors. As expected, total precipitation is not changed downwind of St. Louis by the

interactions of topography and urban momentum flux (Fig. 22c).

5. Summary and conclusions

A case study of deep, moist convection over St. Louis, Missouri, was chosen for numerical investigation of possible urban-enhanced precipitation. The climatological conditions associated with the greatest number of urban-enhanced storms were matched in this case study, making the case relevant to many situations occurring in moist, temperate urban areas. The hypotheses investigated were those that explained enhanced convection by surface convergence produced by both the urban heat island and increased roughness of the urban surface and topography.

RAMS explicitly simulated deep, moist convection. Sophisticated surface boundary conditions, including a generalized urban canyon scheme for dense urban land use, were included. The model was compared with observational data, exhibiting suitable performance. All

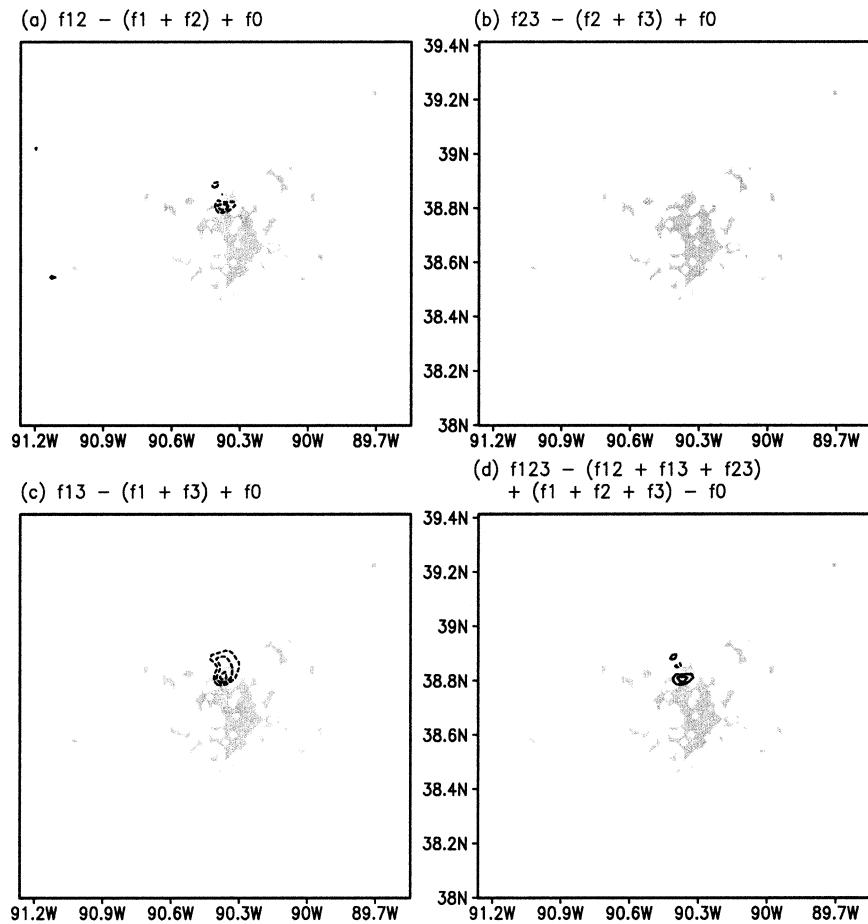


FIG. 21. Storm initiation due to (a) \hat{f}_{12} , (b) \hat{f}_{23} , (c) \hat{f}_{13} , and (d) \hat{f}_{123} at 1900 UTC. Plotted are contours (interval of 10 mm) of vertically integrated condensate. Dashed contours indicate negative values, whereas solid contours indicate positive values. LEAF-2 class 30 is shaded to indicate the position of St. Louis.

model simulations were initialized at 0000 UTC on 8 June 1999 to foster model spinup time and run for 24 h through the course of a convective event.

Also, the control simulation worked reasonably well in developing a heat island and convection. The nature of the St. Louis heat island was consistent with previous studies over St. Louis and other cities. Boundary layer doming was prevalent over the city, along with enhanced boundary layer convection. The boundary layer advected downwind of St. Louis. This led to convection erupting on the downwind edge of the city. Convection initiated later than it did in radar observations, but the positioning of storms corresponded favorably with radar data.

Sensitivity experiments studied the importance of convergence hypotheses. Differences in the behavior of the urban heat island and convective initiation are large between two urban schemes. The standard LEAF-2 version, which does not account for many features of the 3D city, produces storms downwind of the city 1 h earlier than TEB. Topographic features contribute to

convective development, especially southwest of St. Louis. Topographic circulations leading to storm development appear to be associated with slope–valley flows. The urban heat island circulation plays the largest role in initiating thunderstorms. Its convergence zone forms downwind of the city, leading to sufficient vertical motion to force a storm. Momentum flux generated over the city was not sufficient for storm initiation. Its convergence zone occurred on the windward side of the city. Feedbacks between the momentum flux and energy fluxes cause substantial modification in urban circulations. Momentum flux, created by the urban area, slowed environmental wind and wind driven by the heat island and ensuing circulation. As a result, downwind convergence was dampened. This phenomenon led to later downwind convective development. Any time convection was initiated downwind of St. Louis because of urban effects, the 6-h total precipitation was considerably increased downwind, agreeing with observational analyses. Given the considerable interactions in the

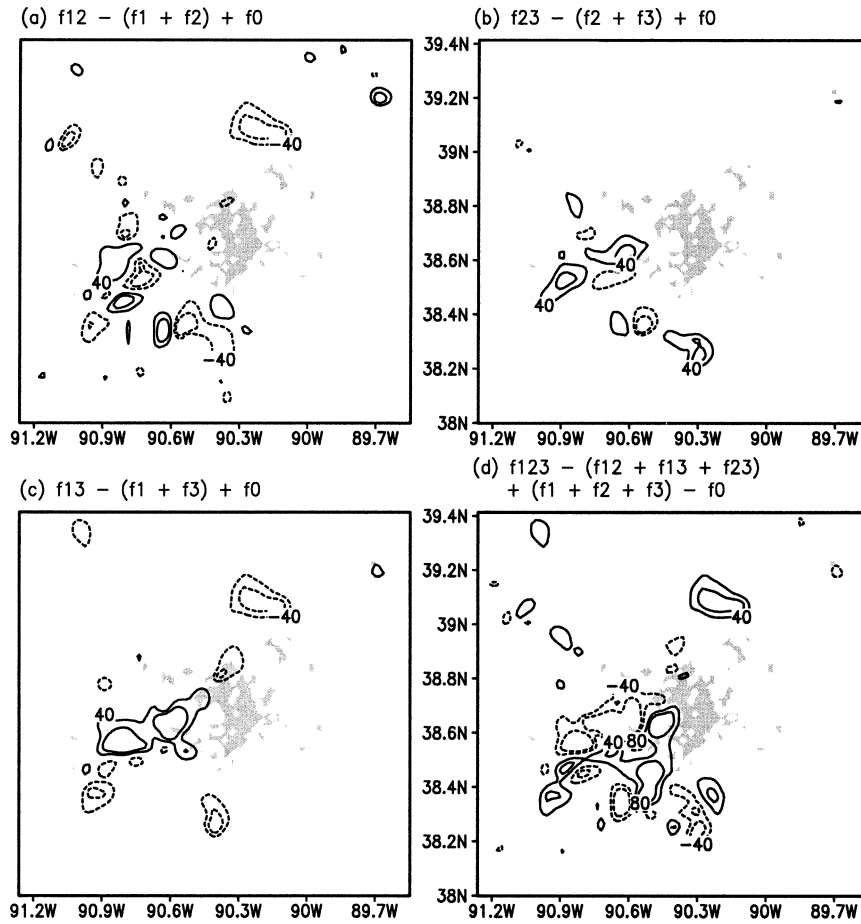


FIG. 22. Total precipitation due to (a) \hat{f}_{12} , (b) \hat{f}_{23} , (c) \hat{f}_{13} , and (d) \hat{f}_{123} at 0000 UTC. Plotted are contours (interval of 40 mm) of total precipitation. Dashed contours indicate negative values, whereas solid contours indicate positive values. LEAF-2 class 30 is shaded to indicate the position of St. Louis.

model solution, it is questionable how well the hypotheses of convergence can be separated in an observational study.

A variety of questions await future work in simulating urban-enhanced thunderstorms. First, the parameterization of the surface is a challenge that warrants improvement. As computing improves, increased resolution and detail of the surface in simulations will be necessary to properly assess surface forcings. The current study applies uniform, average urban values to the parameters of TEB to approximate all densely urban portions of the model domain. As grid spacing decreases, variations in the TEB parameters will be necessary in the future. Complete anthropogenic heat flux and building characteristics inventories over St. Louis and other cities will also improve heat island simulations.

When contending with urban-enhanced convection, two varieties of modeling studies may be carried out: idealized simulations and case studies. Both have the ability to examine a myriad of convective situations. The current study investigates a common situation for

temperate, midlatitude cities in the summer, where convection is forced in an environment free of significant large-scale dynamical factors. The next logical step is to repeat similar experiments with various common convective regimes, especially mesoscale convective systems (MCSs) and, in particular, nocturnal MCSs (see observations of Changnon and Huff 1986).

Last, the hypothesis of microphysical influences on storms has yet to be properly investigated. To the best of the authors' knowledge, the area of microphysical interactions with storms is barely touched upon by urban modeling studies. Certainly the experiments in this study can be extended to studies of urban aerosol influences on microphysical processes. The important pollutant aerosols to examine include variations in concentrations of cloud-condensation nuclei, giant cloud-condensation nuclei, and ice-forming nuclei.

Acknowledgments. Our gratitude is extended to Valery Masson (Centre National de Recherches Météorologiques) for use of the Town Energy Budget. We

thank Liz Page, Ray McAnelly, and Curtis Marshall for meteorological data. We are grateful for the 1-km-resolution version of the NLCD provided by Dr. Zhiqiang Gao. The assistance of Jill Schaefer and Brenda Thompson is greatly appreciated. Comments by three reviewers helped to clarify this manuscript. This research was supported by the National Science Foundation under Grant No. ATM-9900929. Part of this work is from a thesis submitted by the first author to the academic faculty of Colorado State University in partial fulfillment of the requirements for the degree of Master of Science.

REFERENCES

- Baik, J.-J., and Y.-H. Kim, 2001: Dry and moist convection forced by an urban heat island. *J. Appl. Meteor.*, **40**, 1462–1475.
- Balling, R. C., and S. W. Brazel, 1987: Recent changes in Phoenix, Arizona, summertime diurnal precipitation patterns. *Theor. Appl. Climatol.*, **38**, 50–54.
- Bornstein, R., and Q. Lin, 2000: Urban heat islands and summertime convective thunderstorms in Atlanta: Three case studies. *Atmos. Environ.*, **34**, 507–516.
- Braham, R. R., 1976: Modification of clouds and weather by a large metropolitan area. Preprints, *Second WMO Scientific Conf. on Weather Modification*, Boulder, CO, WMO, 435–442.
- Changnon, S. A., 1981: *METROMEX: A Review and Summary. Meteor. Monogr.*, No. 18, Amer. Meteor. Soc., 181 pp.
- , and F. A. Huff, 1986: The urban-related nocturnal rainfall anomaly at St. Louis. *J. Climate Appl. Meteor.*, **25**, 1985–1995.
- Chen, C., and W. R. Cotton, 1983: A one-dimensional simulation of the stratocumulus-capped mixed layer. *Bound.-Layer Meteor.*, **25**, 289–321.
- Cotton, W. R., and Coauthors, 2003: RAMS 2001: Current status and future directions. *Meteor. Atmos. Phys.*, **82**, 5–29.
- Craig, K. J., and R. D. Bornstein, 2002: MM5 simulations of urban induced convective precipitation over Atlanta. Preprints, *Fourth Symp. on the Urban Environment*, Norfolk, VA, Amer. Meteor. Soc., 5–6.
- Dickinson, R. E., A. Henderson-Sellers, P. J. Kennedy, and M. F. Wilson, 1986: Biosphere–Atmosphere Transfer Scheme (BATS) for the NCAR Community Climate Model. NCAR Tech. Rep. NCAR/TN275 + STR, 69 pp.
- Hjelmfelt, M. R., 1982: Numerical simulation of the effects of St. Louis on mesoscale boundary-layer airflow and vertical air motion: Simulations of urban vs non-urban effects. *J. Appl. Meteor.*, **21**, 1239–1257.
- Huff, F. A., and J. L. Vogel, 1978: Urban, topographic and diurnal effects on rainfall in the St. Louis region. *J. Appl. Meteor.*, **17**, 565–577.
- Jauregui, E., and E. Romales, 1996: Urban effects on convective precipitation in Mexico City. *Atmos. Environ.*, **30**, 3383–3389.
- Johnson, R. H., and J. J. Toth, 1982: Topographic effects and weather forecasting in the Colorado PROFS mesonet network area. Preprints, *Ninth Conf. on Weather Forecasting and Analysis*, Seattle, WA, Amer. Meteor. Soc., 440–444.
- Klemp, J. B., and R. B. Wilhelmson, 1978: The simulation of three-dimensional convective storm dynamics. *J. Atmos. Sci.*, **35**, 1070–1096.
- Lee, T. J., 1992: The impact of vegetation on the atmospheric boundary layer and convective storms. Ph.D. dissertation, Colorado State University, 137 pp.
- Masson, V., 2000: A physically-based scheme for the urban energy budget in atmospheric models. *Bound.-Layer Meteor.*, **94**, 357–397.
- Morris, C. J. G., I. Simmonds, and N. Plummer, 2001: Quantification of the influences of wind and cloud on the nocturnal urban heat island of a large city. *J. Appl. Meteor.*, **40**, 169–182.
- Oke, T. R., 1988: The urban energy balance. *Prog. Phys. Geogr.*, **12**, 471–508.
- Rogers, E., T. L. Black, D. G. Deaven, G. J. DiMego, Q. Zhao, M. E. Baldwin, N. W. Junker, and Y. Lin, 1996: Changes to the operational “early” eta analysis/forecast system at the National Centers for Environmental Prediction. *Wea. Forecasting*, **11**, 391–416.
- Spangler, T. C., and R. A. Dirks, 1974: Mesoscale variations of the urban mixing height. *Bound.-Layer Meteor.*, **6**, 428–441.
- Stein, U., and P. Alpert, 1993: Factor separation in numerical simulations. *J. Atmos. Sci.*, **50**, 2107–2115.
- Thielen, J., W. Wobrock, A. Gadian, P. G. Mestayer, and J.-D. Creutin, 2000: The possible influence of urban surfaces on rainfall development: A sensitivity study in 2D in the meso-gamma-scale. *Atmos. Res.*, **54**, 15–39.
- Walko, R. L., and Coauthors, 2000: Coupled atmosphere–biophysics–hydrology models for environmental modeling. *J. Appl. Meteor.*, **39**, 931–944.